BONN-TH-2015-12

R-Parity Violation and Light Neutralinos at SHiP and the LHC

Jordy de Vries,[1,*] Herbi K. Dreiner,[2,†] and Daniel Schmeier[2,‡]

[1] *Institute for Advanced Simulation, Institut für Kernphysik, Jülich Center for Hadron Physics, Forschungszentrum Jülich, D-52425 Jülich, Germany*
[2] *Physikalisches Institut der Universität Bonn, Bethe Center for Theoretical Physics, Nußallee 12, 53115 Bonn, Germany*

We study the sensitivity of the proposed SHiP experiment to the LQD operator in R-Parity violating supersymmetric theories. We focus on single neutralino production via rare meson decays and the observation of downstream neutralino decays into charged mesons inside the SHiP decay chamber. We provide a generic list of effective operators and decay width formulae for any λ' coupling and show the resulting expected SHiP sensitivity for a widespread list of benchmark scenarios via numerical simulations. We compare this sensitivity to expected limits from testing the same decay topology at the LHC with ATLAS.

I. INTRODUCTION

Supersymmetry [1–3] is the unique extension of the external symmetries of the Standard Model of elementary particle physics (SM) with fermionic generators [4]. Supersymmetry is necessarily broken, in order to comply with the bounds from experimental searches. To solve the hierarchy problem [5, 6], the masses of the supersymmetric partners of the SM fields should be lighter than 1-10 TeV, with a clear preference for lighter fields, see for example [7–11]. All experimental searches for supersymmetric particles have hitherto been unsuccessful. The LHC sets limits on the strongly interacting sparticles, the squarks and gluinos, of order 1 TeV, see for example [12, 13]. However the limits on the only electroweak interacting particles, such as the sleptons, the neutralinos and the charginos, are significantly weaker [14, 15]. In fact, as has been discussed in the literature there is currently *no lower mass bound* on the lightest supersymmetric particle (LSP) neutralino, which is model independent [16, 17]. The limits from LEP can easily be avoided, and in particular, a massless neutralino is still allowed, for sufficiently heavy selectrons and squarks [18]. We discuss this in more detail below, in Sec. III.

We are here interested in the possibilities of searching for a light neutralino, up to masses of about 10 GeV. Already for a slepton mass of 150 GeV there is no sensitivity via the process $e^+e^- \to \tilde{\chi}_1^0\chi_1^0\gamma$ from LEP data [19], see also [20, 21]. Since mass reach is not a factor, one might suspect that the high intensity facilities used as B-factories, would be more sensitive, but this is also not the case [19].

In order to avoid over-closing the universe [22–24], a 10 GeV or lighter neutralino must decay via R-parity violating operators [25]. If the R-parity violating couplings are not too small, in this case, the most promising method to search for a light neutralino, is via the production of mesons. The rate for the latter is so high, that the subsequent rare decay of the meson to the light neutralino via (an) R-parity violating operator(s) can be searched for [26–28]. This is analogous to the production of neutrinos via π or K-mesons.

For a neutralino in the mass range of about 0.5 - 5 GeV, the newly proposed SHiP experimental facility [29] seems ideal. It will consist of a high intensity 400 GeV proton beam from the CERN SPS incident on a fixed target. 63.8 m down beam line there will a detector for long-lived heavy neutral particles. Two of us (HKD, DS) have performed a preliminary analysis in [30], for a small set of R-parity violating operators: the decay $D^+ \to \tilde{\chi}_1^0\,\ell_i^+$ via the operator $\lambda'_{i21}L_iQ_2\bar{D}_1$, and the decays $\tilde{\chi}_1^0 \to (K^0\nu; K^\mp\ell_i^\pm)$ via $\lambda'_{i21,i21}$. It is the purpose of this paper to extend this to all possible production modes and decay channels, and to determine the search sensitivity of the SHiP experiment. As an example, in earlier work [26], the production of B-mesons at NuTeV was considered. The mesons could decay as $B_{d,s}^0 \to \tilde{\chi}_1^0\,\nu$ or $B^\pm \to \tilde{\chi}_1^0\,\ell_i^\pm$ via λ'_{i13}. The neutralinos could decay via the $L_iQ_1\bar{D}_3$ operators, or purely leptonically via $L_iL_j\bar{E}_k$ operators. These scenarios can also be tested at SHiP, where a sufficiently large number of B-type mesons is expected and we will show the sensitivity reach to the $LQ\bar{D}$ operators here.

This paper is organized as follows. In Sec. II, we briefly review supersymmetry with broken R-parity. We also discuss the bounds on the operators relevant to our analysis. Constraints on the neutralino mass and motivations for the possibility of a very light neutralino follow in Sec. III. In Sec. IV we discuss the relevant neutralino production and decay channels we expect to be most relevant for SHiP observations of R-parity violation (RPV). In Sec. V we set up the effective field theory need to compute the relevant meson and neutralino decays and compute the latter in general fashion. With these results at hand, we specialize to the SHiP set-up in Sec. VI and discuss under what circumstances a neutralino could be detected. In Sec. VII we explain the methodology of

* j.de.vries@fz-juelich.de
† dreiner@uni–bonn.de
‡ daschm@th.physik.uni–bonn.de

our numerical study. The discussion of the sensitivity of the SHiP experiment to the existence of light, but unstable, neutralinos in several benchmark scenarios is given in Sec. VIII. In Sect. IX, we discuss an estimate for possible effects of our benchmark scenarios at the LHC. We conclude in Sect. X.

II. R-PARITY VIOLATION

A. Introduction

The minimal supersymmetric extension of the SM requires the introduction of an additional Higgs doublet. The minimal set of pure matter couplings are then encoded in the minimal supersymmetric SM (MSSM) superpotential

$$W_{\rm MSSM} = (h_E)_{ij} L_i H_d \bar{E}_j + (h_D)_{ij} Q_i H_d \bar{D}_j + (h_U)_{ij} Q_i H_u \bar{U}_j + \mu H_d H_u \,. \quad (1)$$

Here $h_{E,D,U}$ are dimensionless 3×3 coupling matrices. The Higgs mixing μ has mass dimension one. This superpotential is equivalent to imposing the discrete $\mathbf{Z}_2$ symmetry R-parity [31], or the $\mathbf{Z}_6$ proton hexality [32], and results in a stable proton. Both are discrete gauge anomaly-free, ensuring stability under potential quantum gravity corrections [33]. A model restricted to the superpotential $W_{\rm MSSM}$ is called R-parity conserving. The advantage is that the LSP, usually the lightest neutralino, is an automatic WIMP dark matter candidate [34]. However, no such dark matter has been observed to-date, motivating the search for other forms of supersymmetry.

Instead in R-parity violating models, there are further possible terms in the superpotential

$$W_{\rm RPV} = W_{LV} + W_{BV} \,, \quad (2)$$

$$W_{\rm LV} = \lambda_{ijk} L_i L_j \bar{E}_k + \lambda'_{ijk} L_i Q_j \bar{D}_k + \kappa_i L_i H_u \,, \quad (3)$$

$$W_{\rm BV} = \lambda''_{ijk} \bar{U}_i \bar{D}_j \bar{D}_k \,. \quad (4)$$

Imposing the discrete $\mathbf{Z}_3$ symmetry baryon triality [32, 35], the lepton-number violating terms in $W_{\rm LV}$ remain. The proton remains stable, since baryon-number is conserved, however the neutralino LSP is unstable and is no longer a dark matter candidate. This can be solved by introducing the axion to solve the problem of CP-violation in QCD. The supersymmetric partner, the axino, is then automatically a good dark matter candidate [36–39] and light neutrino masses are also generated automatically [40–44]. We thus consider this a well-motivated model to investigate. At a given energy scale the bilinear terms $\kappa_i L_i H_u$ can be rotated away, even for complex κ_i, μ [40, 41, 45]. This leaves us with the tri-linear couplings λ_{ijk} and λ'_{ijk}. In this work we focus on the latter couplings as they lead to neutralino production via the decays of mesons.

B. Bounds on R-parity Violating Couplings

The operators $L_i Q_j \bar{D}_k$ which we investigate here all violate lepton number; thus there are strict bounds on the coupling constants λ'_{ijk}, see for example the reviews [46–50]. We briefly summarize here the existing bounds on the specific operators which we investigate in our benchmark scenarios in Sec. VIII. For our results on the sensitivity reach of SHiP, we focus on the cases λ'_{1jk}, involving final state electrons, and λ'_{31k}, which produces tau leptons. However, experimentally final state muons should be testable at least as well as electrons. We thus also present the corresponding bounds on the couplings λ'_{2jk}, which are typically weaker. We take most of the numbers from the most recent review [50].

$$\lambda'_{112} < 0.03 \, \frac{m_{\tilde{s}_r}}{100\,\text{GeV}}, \qquad \lambda'_{212} < 0.06 \, \frac{m_{\tilde{s}_R}}{100\,\text{GeV}}. \quad (5)$$

$$\lambda'_{121} < 0.2 \, \frac{m_{\tilde{c}_L}}{100\,\text{GeV}}, \qquad \lambda'_{221} < 0.1 \, \frac{m_{\tilde{d}_R}}{100\,\text{GeV}}, \quad (6)$$

$$\lambda'_{122} < 0.2 \, \frac{m_{\tilde{c}_L}}{100\,\text{GeV}}, \qquad \lambda'_{222} < 0.1 \, \frac{m_{\tilde{s}_R}}{100\,\text{GeV}}, \quad (7)$$

$$\lambda'_{131} < 0.03 \, \frac{m_{\tilde{t}_L}}{100\,\text{GeV}}, \qquad \lambda'_{231} < 0.18 \, \frac{m_{\tilde{b}_L}}{100\,\text{GeV}}, \quad (8)$$

$$\lambda'_{312} < 0.06 \, \frac{m_{\tilde{s}_R}}{100\,\text{GeV}}, \quad (9)$$

$$\lambda'_{313} < 0.06 \, \frac{m_{\tilde{t}_L}}{100\,\text{GeV}}, \quad (10)$$

The bound on λ'_{231} is from [48], as there is no bound quoted in [50]. Assuming an experimental neutrino mass bound $m_\nu < 1\,\text{eV}$ results in a bound of approximately $\lambda'_{122,222} < 0.01\sqrt{\tilde{m}/100\,\text{GeV}}$ [40, 48, 51]. This is however model dependent, as we know there must be further, possibly off-diagonal, contributions to the neutrino mass matrix.

III. A LIGHT NEUTRALINO

The best lower mass limit on the lightest supersymmetric particle (LSP) neutralino is from LEP [17]

$$m_{\tilde{\chi}^0_1} > 46\,\text{GeV}. \quad (11)$$

This uses the LEP-II chargino search to restrict the range of μ and the SU(2) soft breaking gaugino mass parameter M_2 and then assumes the supersymmetric GUT relation

$$M_1 = \frac{5}{3} \tan^2\theta_W \, M_2 \approx \frac{1}{2} M_2 \,, \quad (12)$$

where M_1 is the $\text{U}(1)_Y$ soft breaking gaugino mass. The LEP-II searches translate into $M_1 \gtrsim 50\,\text{GeV}$. Performing the Takagi diagonalization of the neutralino mass matrix [52] and scanning the parameters M_1, M_2, μ, $\tan\beta$ over the allowed ranges, results in the bound of Eq. (11).

If the GUT assumption is dropped and M_1, M_2 are independent parameters, setting the determinant of the neutralino mass matrix to zero results in the relation

$$M_1 = \frac{M_2 M_Z^2 \sin(2\beta)\sin^2\theta_{\rm W}}{\mu M_2 - M_Z^2 \sin(2\beta)\cos^2\theta_{\rm W}}\,. \tag{13}$$

For real parameters this equation can always be solved [16]. Thus for given values of μ, M_2, and $\tan\beta$ there is always a mass-zero singular value [52], and thus a massless neutralino state. A neutralino lighter than $\mathcal{O}(10\,\text{GeV})$ is dominantly bino and does not couple directly to the Z^0-boson. Thus the bounds on a light neutralino from the invisible Z^0-width are avoided [19]. In fact to our knowledge all laboratory bounds are avoided [16].

The strictest mass bounds on a stable, light neutralino are astrophysical. Supernova [18, 53] or white dwarf cooling [54], give a lower mass bound: $m_{\tilde\chi_1^0} \gtrsim 250\,\text{MeV}$, for selectron masses around 320 GeV. In this case, too few neutralinos are produced, due to Boltzmann suppression, as the supernova temperature is about 30 MeV. A *massless* neutralino is allowed for selectron masses above about 1275 GeV or below 320 GeV. For $M_{\tilde e} > 1275\,\text{GeV}$ also too few neutralinos are produced. For $M_{\tilde e} < 320\,\text{GeV}$ the neutralinos are trapped in the supernova, similar to neutrinos and must be included in the full supernova simulation. Since this has not been done to-date, the supernova does not give a reliable bound in this region.

Cosmologically the Cowsik-McClelland bound [55] on a very light neutrino translates into the *upper* neutralino mass bound [16]

$$M_{\tilde\chi_1^0} < 0.7\,\text{eV}\,. \tag{14}$$

The neutralino in this case provides hot dark matter, but not enough to negatively affect structure formation. The observed dark matter density must then originate elsewhere, for example from the axino.

Requiring the lightest neutralino to provide the observed dark matter results in a *lower* mass bound, the Lee–Weinberg bound [56]. The proper bound is obtained by scanning over the allowed supersymmetric parameter space, while dropping the relation in Eq. (12). This is thus an on–going process [22]. The most recent bound including the Higgs–discovery data and also constraints from stau searches gives [24, 57–59]

$$M_{\tilde\chi_1^0} > 24\,\text{GeV}\,. \tag{15}$$

Therefore the mass range

$$0.7\,\text{eV} < M_{\tilde\chi_1^0} < 24\,\text{GeV}\,, \tag{16}$$

is excluded for a stable neutralino LSP as it gives too much dark matter. A neutralino LSP in this mass range is only allowed if it decays, *i.e.* R-parity is violated.

IV. LIGHT NEUTRALINOS AT SHIP

A. The SHiP Setup

We present some details of the SHiP setup that are relevant to our analysis. The SHiP proposal [29] is not definitive yet. The plan is to employ the 400 GeV proton beam at CERN in the fixed-target mode. This yields a center-of-mass energy of roughly 27 GeV, sufficient to produce D and B mesons. Over the lifetime of the experiment a total of $2\cdot10^{20}$ protons on target are foreseen. Such a large event yield is expected to be achievable by *e.g.* a hybrid target consisting of tungsten and titanium-zirconium doped molybdenum alloy.

A major motivation for the SHiP experiment is to observe new, weakly-interacting particles with long lifetimes. Such particles could be produced via proton-target-collisions and propagate for finite distances of the order tens of meters before decaying back into Standard Model pairs. For that purpose, a decay volume is located 68.8 m behind the target. It has a cylindrical shape with a total length of 60 m, however with the first 5 m dedicated for background suppression vetoes. Furthermore, the decay region has an elliptic face front with semi-axes 5 m and 2.5 m. We sketch this setup in Fig. 2. A spectrometer and a calorimeter system positioned behind the decay volume can identify the visible final state particles that are potentially produced when a hidden particle decays.

B. Production and Decay of Neutralinos via R-Parity Violation

Since the goal is to investigate the light supersymmetric neutralino, one might consider their direct production. However, in Ref. [26] using the Monte Carlo program `HERWIG 6.2` [60] the pair production of neutralinos in a proton fixed target experiment

$$p + p \to \tilde\chi_1^0 \tilde\chi_1^0 + X\,, \tag{17}$$

was shown to be three orders of magnitude too low at the NuTeV experiment, for squark masses of 100 GeV. Since the light neutralino is almost pure bino, the dominant production mode is via t-channel squark exchange, and the cross section goes as $1/m_{\tilde q}^4$. At SHiP it is planned to have 100 times more protons on target than at NuTeV. However, the lower squark mass bound is now also about a factor of 10 stricter. One would thus expect a further two orders of magnitude suppression, making this a hopeless endeavour also at SHiP.

As in Ref. [26], we instead consider the production of mesons M, which can have a very large production cross section. On rare occasions these mesons can decay to the neutralino LSP and a neutral or charged lepton l via

$$\begin{aligned} p + p &\to M + X \\ M &\to \tilde\chi_1^0 + l. \end{aligned} \tag{18}$$

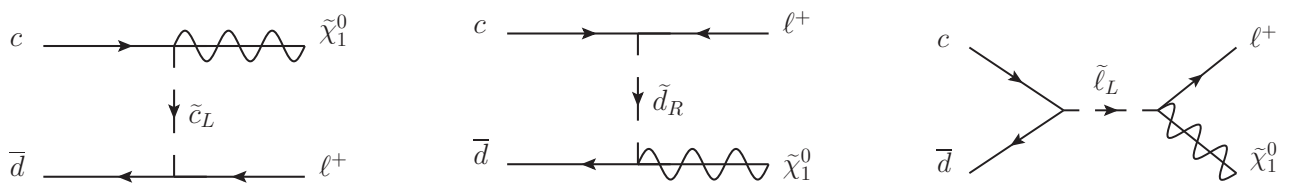

FIG. 1. Relevant Feynman Diagrams for $D^+ \to \tilde{\chi}_1^0 + \ell^+$

At SHiP energies, with a 400 GeV proton beam we expect (next to the production of light mesons containing up, down, or strange quarks) high production rates for charmed mesons, and somewhat lower rates for B-mesons. As we discuss below, for example over the lifetime of SHiP about 4.8×10^{16} $D^{\pm}$-mesons are expected. Thus even very rare decays can be probed. Individual $L_i Q_a \bar{D}_b$ R-parity violating operators allow for leptonic decays of mesons. As an example the tree-level Feynman diagrams for the decay

$$D^+ \to \tilde{\chi}_1^0 + \ell_i^+, \, i = 1, 2 \, . \tag{19}$$

are given in Fig. 1, for $a = 2, b = 1$. In this specific example the light neutralino can decay via the same R-parity violating operator:

$$\tilde{\chi}_1^0 \to (\nu \, K_{S/L}^0; \, \bar{\nu} \, \bar{K}_{S/L}^0) \, . \tag{20}$$

Both sets of decays are possible, as the neutralino is a Majorana fermion. For small values of the coupling λ'_{i21} and given that the neutralino must be lighter than the D^+ meson, the neutralino lifetime can be long enough to decay downstream in the SHiP detector.

V. EFFECTIVE INTERACTIONS: LEPTON-NEUTRALINO-MESON

In this section, we discuss the R-parity violating effective interactions between a meson, a lepton, and a neutralino. These interactions are relevant for both the production and the decay of the neutralino and are necessary to determine the possible signatures at SHiP, as in Eqs. (19),(20). We focus on the operators $\lambda'_{iab} L_i Q_a \bar{D}_b$ where i denotes the leptonic generation index and a and b the quark generation indices. The index b is always associated with a down-like $SU(2)$ singlet quark, whereas the index a can refer to either an up-like or down-like $SU(2)$ doublet quark. If a is up-like then i corresponds to a charged lepton, *i.e.* electron, muon, or tau, whereas if a is down, i corresponds to a neutrino.

A. The Formalism

The interaction Lagrangian due to $\lambda'_{iab} L_i Q_a \bar{D}_b$ is given in terms of four-component fermions by

$$\begin{aligned} \mathcal{L} \supset \lambda'_{iab} \Big[& (\overline{\nu_i^c} P_L d_a) \widetilde{d}_{bR}^* + (\overline{d_b} P_L \nu^i) \widetilde{d}_{aL} + (\overline{d_b} P_L d_a) \widetilde{\nu}_{iL} \Big] \\ & - \lambda'_{iab} \Big[(\overline{u_a^c} P_L \ell^i) \widetilde{d}_{b_R}^* + (\overline{d_b} P_L u_a) \widetilde{\ell}_{iL} + (\overline{d_b} P_L \ell^i) \widetilde{u}_{aL} \Big] \\ & + \text{h.c.} \end{aligned} \tag{21}$$

Here, $d_{a,b}$, u_a, ν_i, ℓ_i denote the down-like quark, up-like quark, neutrino, and charged lepton fields, respectively. The tilde denote the corresponding supersymmetric scalar partners. The dominant contribution to the R-parity violating decay of a meson typically proceeds at tree-level via operators associated with the Feynman diagrams as shown in Fig. 1. Thus we also need the standard supersymmetric fermion-sfermion-neutralino vertices. We assume that the sfermion mixing is identical to the fermion mixing such that their contributions to the gauge couplings cancel. As we consider a dominantly bino LSP neutralino, $\tilde{\chi}_1^0$, we only take chirality-conserving terms into account

$$\begin{aligned} \mathcal{L} \supset \quad & g_{\tilde{u}_{aL}} (\overline{\widetilde{\chi}_1^0} P_L u_a) \widetilde{u}_{a_L}^* + g_{\tilde{d}_{aL}} (\overline{\widetilde{\chi}_1^0} P_L d_a) \widetilde{d}_{a_L}^* \\ & + g_{\tilde{l}_{i_L}} (\overline{\widetilde{\chi}_1^0} P_L \ell_i) \widetilde{\ell}_{iL}^* + g_{\tilde{\nu}_{i_L}} (\overline{\widetilde{\chi}_1^0} P_L \nu_i) \widetilde{\nu}_{i_L}^* \\ & + g_{\tilde{d}_R}^* (\overline{d} P_L \widetilde{\chi}_1^0) \widetilde{d}_R + \text{h.c.} \end{aligned} \tag{22}$$

We assume that the sfermion masses are significantly larger than the momentum exchange of the process. Thus the sfermions can be integrated out, resulting at tree-level in the low-energy effective four-fermion Lagrangian for both the production and decay of the neutralino:

$$\begin{aligned} \mathcal{L} \supset \lambda'_{iab} \Bigg[& \frac{g_{\tilde{d}_{bR}}^*}{m_{\tilde{d}_{b_R}}^2} (\bar{d}_b P_L \tilde{\chi}_1^0) (\overline{\nu_i^c} P_L d_a) \\ & - \frac{g_{\tilde{d}_{bR}}^*}{m_{\tilde{d}_{b_R}}^2} (\bar{d}_b P_L \tilde{\chi}_1^0) (\overline{u_a^c} P_L \ell_i) + \frac{g_{\tilde{d}_{aL}}}{m_{\tilde{d}_{a_L}}^2} (\overline{\widetilde{\chi}_1^0} P_L d_a) (\overline{d_b} P_L \nu_i) \\ & - \frac{g_{\tilde{u}_{aL}}}{m_{\tilde{u}_{a_L}}^2} (\overline{\widetilde{\chi}_1^0} P_L u_a) (\overline{d_b} P_L \ell_i) + \frac{g_{\tilde{\nu}_{iL}}}{m_{\tilde{\nu}_{i_L}}^2} (\overline{\widetilde{\chi}_1^0} P_L \nu_i) (\overline{d_b} P_L d_a) \\ & - \frac{g_{\tilde{\ell}_{iL}}}{m_{\tilde{\ell}_{i_L}}^2} (\overline{\widetilde{\chi}_1^0} P_L \ell_i) (\overline{d_b} P_L u_a) \Bigg] + \text{h.c.} \end{aligned} \tag{23}$$

We have omitted the terms involving pairs of neutralinos, which are most likely not relevant at SHiP, see [28]. Sim-

ilarly, we have dropped interactions involving four SM fermions, see [46].

For pure bino interactions, the coupling constants g_X are family independent [61]

$$g_{\tilde{\ell}_{iL}} = g_{\tilde{\ell}_L} = +\frac{g_2}{\sqrt{2}}\tan\theta_W, \tag{24}$$

$$g_{\tilde{\nu}_{iL}} = g_{\tilde{\nu}_L} = +\frac{g_2}{\sqrt{2}}\tan\theta_W, \tag{25}$$

$$g_{\tilde{u}_{aL}} = g_{\tilde{u}_L} = -\frac{g_2}{3\sqrt{2}}\tan\theta_W, \tag{26}$$

$$g_{\tilde{d}_{aL}} = g_{\tilde{d}_L} = +\frac{5g_2}{3\sqrt{2}}\tan\theta_W, \tag{27}$$

$$g_{\tilde{d}_{bR}} = g_{\tilde{d}_R} = -\frac{2g_2}{3\sqrt{2}}\tan\theta_W, \tag{28}$$

Here, θ_W denotes the electroweak mixing angle and g_2 the Standard Model SU(2) gauge coupling.

Using chiral Fierz identities (*e.g.* [62]), one can rearrange the four-fermion interactions in Eq. (23) such that each term factorizes in a neutralino-lepton current and a quark-bilinear:

$$\begin{aligned}(\bar{\psi}_1 P_{\substack{L\\R}}\eta_2)(\bar{\eta}_1 P_{\substack{L\\R}}\psi_2) = &-\frac{1}{2}(\bar{\psi}_1 P_{\substack{L\\R}}\psi_2)(\bar{\eta}_1 P_{\substack{L\\R}}\eta_2)\\ &-\frac{1}{4}(\bar{\psi}_1\sigma^{\mu\nu}\psi_2)(\bar{\eta}_1\sigma_{\mu\nu}\eta_2)\\ &\pm\frac{i}{8}\epsilon^{\mu\nu\rho\sigma}(\bar{\psi}_1\sigma_{\mu\nu}\psi_2)(\bar{\eta}_1\sigma_{\rho\sigma}\eta_2),\end{aligned} \tag{29}$$

with $\sigma^{\mu\nu} \equiv i/2\,[\gamma^\mu,\gamma^\nu]$ and $\epsilon^{0123} = 1$. $\psi_{1,2}$, $\eta_{1,2}$ denote four component fermions. Making use of these identities and applying $\overline{\psi^{\mathcal{C}}}P_{L/R}\eta = \overline{\eta^{\mathcal{C}}}P_{L/R}\psi$ in combination with the Majorana identity $\chi^{\mathcal{C}} = \chi$ for the neutralino, Eq. (23) can be written as the sum of the following four interactions:

$$(\overline{\widetilde{\chi}^0}P_L\nu_i)(\overline{d_b}P_L d_a)\times \underbrace{\lambda'_{iab}\Big(\frac{g_{\tilde{\nu}_L}}{m^2_{\tilde{\nu}_{i_L}}} - \frac{1}{2}\frac{g_{\tilde{d}_L}}{m^2_{\tilde{d}_{a_L}}} - \frac{1}{2}\frac{g^*_{\tilde{d}_R}}{m^2_{\tilde{d}_{b_R}}}\Big)}_{\equiv G^{S,\nu}_{iab}}, \tag{30}$$

$$(\overline{\widetilde{\chi}^0}P_L\ell_i)(\overline{d_b}P_L u_a)\times \underbrace{\lambda'_{iab}\Big(\frac{1}{2}\frac{g_{\tilde{u}_L}}{m^2_{\tilde{u}_{a_L}}} + \frac{1}{2}\frac{g^*_{\tilde{d}_R}}{m^2_{\tilde{d}_{b_R}}} - \frac{g_{\tilde{\ell}_L}}{m^2_{\tilde{\nu}_{i_L}}}\Big)}_{\equiv G^{S,\ell}_{iab}}, \tag{31}$$

$$(\overline{\widetilde{\chi}^0}\sigma^{\mu\nu}\nu_i)(\overline{d_b}\sigma^{\rho\sigma}d_a)\times \underbrace{\lambda'_{iab}\Big(\frac{g_{\tilde{d}_L}}{4m^2_{\tilde{d}_{a_L}}} + \frac{g^*_{\tilde{d}_R}}{4m^2_{\tilde{d}_{b_R}}}\Big)}_{\equiv G^{T,\nu}_{iab}}\Big(g_{\mu\rho}g_{\nu\sigma} - \frac{i\epsilon_{\mu\nu\rho\sigma}}{2}\Big), \tag{32}$$

$$(\overline{\widetilde{\chi}^0}\sigma^{\mu\nu}\ell_i)(\overline{d_b}\sigma^{\rho\sigma}u_a)\times \underbrace{\lambda'_{iab}\Big(\frac{g_{\tilde{u}_L}}{4m^2_{\tilde{u}_{a_L}}} + \frac{g^*_{\tilde{d}_R}}{4m^2_{\tilde{d}_{b_R}}}\Big)}_{\equiv G^{T,\ell}_{iab}}\Big(g_{\mu\rho}g_{\nu\sigma} - \frac{i\epsilon_{\mu\nu\rho\sigma}}{2}\Big), \tag{33}$$

and their hermitean conjugates.

For pseudoscalar mesons composed of anti-quarks $\bar{q}_1$ and quarks q_2, we can connect the quark bilinear vector currents with external meson fields by defining pseudoscalar meson decay constants f_M

$$\langle 0|\bar{q}_1\gamma^\mu\gamma^5 q_2|M(p)\rangle \equiv ip^\mu f_M, \tag{34}$$

where $|M(p)\rangle$ denotes a pseudoscalar meson M with momentum p. The standard current-algebra approximation then predicts

$$\langle 0|\bar{q}_1\gamma^5 q_2|M(p_M)\rangle = i\frac{m_M^2}{m_{q_1}+m_{q_2}}f_M \equiv f_M^S, \tag{35}$$

for the pseudoscalar currents in Eqs. (30) and (31). Here, m_M, m_{q_1} and m_{q_2} are the masses of the meson M and the quarks q_1, q_2, respectively.

The tensor structure in Eqs. (32), (33) does not lead to purely leptonic processes such as $M \to \widetilde{\chi}^0 + l_i$ or $\widetilde{\chi}^0 \to M + l_i$, because a pseudoscalar meson only has one relevant Lorentz-vector, its momentum. Thus the tensor interactions only contribute to higher multiplicity processes such as $M \to \widetilde{\chi}^0 + l_i + M'$, where M' denotes a lighter meson. These are phase space suppressed by two to three orders of magnitude, and we do not consider them here.

Vector mesons have two intrinsic Lorentz vectors, their momentum p^μ and polarization ϵ^μ. The decay constant of a vector meson M^* with mass m_{M^*}, can be defined as

$$\langle 0|\bar{q}_1\gamma^\mu q_2|M^*(p,\epsilon)\rangle \equiv f^V_{M^*}m_{M^*}\epsilon^\mu. \tag{36}$$

Heavy-quark symmetry relates the vector and pseudoscalar constants for mesons containing a heavy quark $f^V_{M^*} \simeq f_M$ [63]. We use this relation for the B and D mesons. For lighter mesons, such as K^* and ϕ, the relation is not accurate and instead we follow Ref. [64], where the vector decay constants are obtained from $M^* \to e^+e^-$ decays.

Similarly we can define the tensor meson constant

$$\langle 0|\bar{q}_1\sigma^{\mu\nu}q_2|M^*(p,\epsilon)\rangle \equiv if^T_{M^*}(p^\mu_M\epsilon^\nu - p^\nu_M\epsilon^\mu). \tag{37}$$

For mesons containing a heavy quark (c or b), heavy-quark symmetry [65] also relates the vector and tensor decay constants $f^T_{M^*} \simeq f^V_{M^*} \simeq f_M$. Because the tensor decay constants are not known in all cases, we also employ this relation for lighter mesons. The additional uncertainties entering via these simplifying assumptions hardly affect the SHiP sensitivity curves on $\lambda'/m^2_{\tilde{f}}$. These range over many orders of magnitude and thus an $\mathcal{O}(40\%)$ correction in a decay constant $f^{S,T,V}_{M^{(*)}}$ does not noticeably change the results presented in the figures in Sec. VIII.

We list the values of the pseudoscalar and vector decay constants we use in Table I in Sect. VIII. In general, we find that neutralinos can interact both with pseudoscalar and vector mesons via different but related effective couplings. In the following analysis we therefore consider both meson types and also show how the inclusion of the latter affects the overall sensitivity.

Potentially fine-tuned models with non-degenerate sfermion masses could lead to a complete cancellation of the individual contributions in Eqs. (30), (31). No sensitivity would be expected in such a scenario if only pseudoscalar mesons were considered in the analysis. However, for a nonzero RPV coupling the effective operators in Eqs. (30)–(33) can not all vanish simultaneously. We hence safely use the simplifying assumption of completely mass degenerate sfermions.

B. Possible Decay Modes

From Eqs. (30)–(33), a single $\lambda'_{iab} L_i Q_a \bar{D}_b$ operator leads to interactions with charged (pseudoscalar or vector) mesons M^+_{ab} of flavour content $(u_a \overline{d_b})$, as well as neutral mesons M^0_{ab} with quark composition $d_a \overline{d_b}$, and their respective charge conjugated equivalents. If $m_{\widetilde{\chi}^0_1} < m_M - m_{l_i}$, the operator opens a decay channel of the meson into the neutralino plus lepton l_i. For example, $M^\pm \to \tilde{\chi}^0_1 \ell^\pm$, or $M^0 \to \tilde{\chi}^0_1 \nu$, $\bar{M}^0 \to \tilde{\chi}^0_1 \bar{\nu}$. Such processes serve as the initial neutralino production mechanism here. In addition, for $m_{\widetilde{\chi}^0_1} > m_M + m_{l_i}$ the neutralino can decay via $\tilde{\chi}^0_1 \to M^+ \ell^-, \bar{M}^- \ell^+$ or $\tilde{\chi}^0_1 \to M^0 \nu, \bar{M}^0 \bar{\nu}$. Such decays can potentially be observed in the SHiP detector.

From the structure of the operators in Eqs.(30)–(33), the definition of the effective couplings and the meson structure constants in Eqs. (35), (37), we obtain the following unpolarized decay widths[1]:

$$\Gamma(M_{ab} \to \widetilde{\chi}^0_1 + l_i) = \frac{\lambda^{\frac{1}{2}}(m^2_{M_{ab}}, m^2_{\widetilde{\chi}^0_1}, m^2_{l_i})}{64\pi m^3_{M_{ab}}} |G^{S,f}_{iab}|^2 (f^S_{M_{ab}})^2 (m^2_{M_{ab}} - m^2_{\widetilde{\chi}^0_1} - m^2_{l_i}), \tag{38}$$

$$\Gamma(M^*_{ab} \to \widetilde{\chi}^0_1 + l_i) = \frac{\lambda^{\frac{1}{2}}(m^2_{M^*_{ab}}, m^2_{\widetilde{\chi}^0_1}, m^2_{l_i})}{3\pi m^3_{M^*_{ab}}} |G^{T,f}_{iab}|^2 (f^T_{M^*_{ab}})^2 \Big[m^2_{M^*_{ab}} (m^2_{M^*_{ab}} + m^2_{\widetilde{\chi}^0_1} + m^2_{l_i}) - 2(m^2_{\widetilde{\chi}^0_1} - m^2_{l_i})^2 \Big], \tag{39}$$

$$\Gamma(\widetilde{\chi}^0_1 \to M_{ab} + l_i) = \frac{\lambda^{\frac{1}{2}}(m^2_{\widetilde{\chi}^0_1}, m^2_{M_{ab}}, m^2_{l_i})}{128\pi m^3_{\widetilde{\chi}^0_1}} |G^{S,f}_{iab}|^2 (f^S_{M_{ab}})^2 (m^2_{\widetilde{\chi}^0_1} + m^2_{l_i} - m^2_{M_{ab}}), \tag{40}$$

$$\Gamma(\widetilde{\chi}^0_1 \to M^*_{ab} + l_i) = \frac{\lambda^{\frac{1}{2}}(m^2_{\widetilde{\chi}^0_1}, m^2_{M^*_{ab}}, m^2_{l_i})}{2\pi m^3_{\widetilde{\chi}^0_1}} |G^{T,f}_{iab}|^2 (f^T_{M^*_{ab}})^2 \Big[2(m^2_{\widetilde{\chi}^0_1} - m^2_{l_i})^2 - m^2_{M^*_{ab}} (m^2_{M^*_{ab}} + m^2_{\widetilde{\chi}^0_1} + m^2_{l_i}) \Big]. \tag{41}$$

Here, l_i either denotes $\ell^\pm_i$ or ν_i, depending on whether M_{ab} is charged or neutral. The phase space function $\lambda^{\frac{1}{2}}(x,y,z) \equiv \sqrt{x^2+y^2+z^2-2xy-2xz-2yz}$. The coefficients G are defined in Eqs. (30)–(33). For each of the above decays there exists a charge-conjugated process with identical decay width. Here we list the most important mesons M_{ab} that participate in each interaction for given a, b

$$\lambda'_{i11} \to \begin{cases} (u\bar{d}) = (\pi^+, \rho^+) \\ (d\bar{d}) = (\pi^0, \eta, \eta', \rho, \omega)\,, \end{cases} \tag{42}$$

$$\lambda'_{i12} \to \begin{cases} (u\bar{s}) = (K^+,\, K^{*+}) \\ (d\bar{s}) = (K^0_L, K^0_S, K^{*0})\,, \end{cases} \tag{43}$$

$$\lambda'_{i13} \to \begin{cases} (u\bar{b}) = (B^+,\, B^{*+}) \\ (d\bar{b}) = (B^0,\, B^{*0})\,, \end{cases} \tag{44}$$

$$\lambda'_{i21} \to \begin{cases} (c\bar{d}) = (D^+,\, D^{*+}) \\ (s\bar{d}) = (K^0_L, K^0_S, K^{*0})\,, \end{cases} \tag{45}$$

$$\lambda'_{i22} \to \begin{cases} (c\bar{s}) = D^+_s,\, D^{*+}_s \\ (s\bar{s}) = \eta,\, \eta',\, \phi \end{cases} \tag{46}$$

$$\lambda'_{i23} \to \begin{cases} (c\bar{b}) = B^+_c,\, B^{*+}_c, \\ (s\bar{b}) = B^0_s,\, B^{*0}_s \end{cases} \tag{47}$$

$$\lambda'_{i31} \to \quad (b\bar{d}) = B^0,\, B^{*0} \tag{48}$$

$$\lambda'_{i32} \to \quad (s\bar{b}) = B^0_s,\, B^{*0}_s \tag{49}$$

$$\lambda'_{i33} \to \quad (b\bar{b}) = \eta_b,\, \Upsilon \tag{50}$$

For light neutral pseudoscalar mesons, mass and flavour eigenstates do not coincide. For our studies this is only relevant for the $\bar{K}^0_{L,S}$, η, and η' mesons (we take

[1] The neutralino decay width in Ref. [30] contains an erroneous sign and misses a factor of 2, which is fixed here in Eq. (40).

Decay constant	Value	Ref.
$f_\eta^{\bar{s}s}$	-142 MeV	[28, 66]
$f_{\eta'}^{\bar{s}s}$	38 MeV	[28, 66]
f_ϕ^V	230 MeV	[64]
f_K	156 MeV	[17]
$f_{K^*}^V$	230 MeV	[64]
f_D, $f_{D^\star}^V$	205 MeV	[17]
f_{D_s}, $f_{D_s^\star}^V$	259 MeV	[17]
f_B	191 MeV	[17]
f_{B_s}	228 MeV	[68]

TABLE I. Values of the pseudoscalar and vector decay constants that are used in the various benchmark scenarios. Definitions of the constants are given in Eqs. (34) and (36). Tensor decay constants are chosen to be equal to the pseudoscalar decay constants.

ϕ to be a pure $(s\bar{s})$ state). For the former, we neglect any CP-violation and define the mass eigenstates $|K_{L/S}\rangle \equiv (|K_0\rangle \pm |\bar{K}_0\rangle)/\sqrt{2}$, where $|K_0\rangle$ and $|\bar{K}_0\rangle$ are flavor eigenstates $(d\bar{s})$ and $(s\bar{d})$, respectively. We can then read off the decay constants from

$$\langle 0|\bar{s}\gamma^\mu\gamma^5 d|K_L^0(p)\rangle = +\langle 0|\bar{d}\gamma^\mu\gamma^5 s|K_L^0(p)\rangle = \frac{ip^\mu f_K}{\sqrt{2}}, \quad (51)$$

$$\langle 0|\bar{s}\gamma^\mu\gamma^5 d|K_S^0(p)\rangle = -\langle 0|\bar{d}\gamma^\mu\gamma^5 s|K_S^0(p)\rangle = \frac{ip^\mu f_K}{\sqrt{2}}, \quad (52)$$

where f_K is the decay constant of the charged kaon as defined in Eq. (34).

For η and η' we consider mixing between the η^0 and η^8 flavor states. We are only interested in the $(\bar{s}s)$ content of these mesons. We follow Refs. [28, 66] and define

$$\langle 0|\bar{s}\gamma^\mu\gamma^5 s|\{\eta,\,\eta'\}(p)\rangle = ip^\mu f_{\{\eta,\,\eta'\}}^{\bar{s}s}\,, \quad (53)$$

and give numerical values in Table I.

For the special cases λ'_{ijj} the radiative neutralino decay is possible [40, 67]

$$\tilde{\chi}_1^0 \to \gamma + (\nu_i,\,\bar{\nu}_i)\,. \quad (54)$$

This is necessarily relevant for very light neutralinos, below the pion mass. We do not know how well this would be visible at SHiP, and do not consider it further here.

VI. OBSERVABLE NEUTRALINOS

With the predicted decay widths at hand we investigate how and under which circumstances R-parity violation can be observed at the SHiP experiment. Each λ' coupling causes at least one type of meson to decay into a neutralino and another charged or neutral lepton, provided it is kinematically allowed. This process serves as the initial neutralino production mechanism at SHiP in our analysis. Given the number N_M of mesons M produced at SHiP and the lifetime τ_M, the expected number of initially produced neutralinos is given by

$$N_\chi^{\text{prod.}} = \sum_M N_M \cdot \Gamma(M \to \tilde{\chi}_1^0 + l) \cdot \tau_M. \quad (55)$$

As apparent from the previous section, for each operator there are both pseudoscalar and vector mesons which can produce neutralinos. However, the lifetimes of a pseudoscalar and the corresponding vector meson of the same quark composition differ by many orders of magnitude. As an example, for the lightest charged charm meson, $D^\pm$, and its vector resonance partner, $D^{*\pm}$, one finds $\tau_{D^{*\pm}}/\tau_{D^\pm} \approx 8 \times 10^{-9}$. Similar ratios appear for kaons and even though the lifetime of vector B-mesons is yet unknown there is no reason to expect largely different behaviour. For the RPV decay widths, however, one finds that $\Gamma(D^{*\pm} \to \tilde{\chi}_1^0 \ell^\pm)/\Gamma(D^\pm \to \tilde{\chi}_1^0 \ell^\pm)$ depends mainly on the ratio of masses and of the effective operator couplings G_T/G_S. Thus, it is hardly larger than 2 orders of magnitude unless one chooses a very peculiar setup of fine-tuned parameters. As the expected number of initial mesons, N_M and N_{M^*}, will also be of roughly the same order, we conclude that if both $M \to \tilde{\chi}_1^0 f$ and $M^* \to \tilde{\chi}_1^0 f$ are kinematically allowed, the contribution from vector meson decays is completely negligible.

In the small mass range $m_M < m_{\tilde{\chi}_1^0} < m_{M^*}$ it might only be the vector mesons that can produce neutralinos in the first place, but by the above arguments and from the results below we expect the neutralino event rates to be far too small to be observable. We therefore ignore any neutralino production via vector meson decays in the following study.

For the neutralinos to be observable, a sufficiently high fraction must decay within the decay chamber of the SHiP experiment. By summing the widths $\Gamma(\tilde{\chi}_1^0 \to Mf)$ of all allowed channels for a given operator, we can derive the proper lifetime of a neutralino given the parameters of the RPV supersymmetric model. Given the kinematical distributions of neutralinos produced via meson decay and knowing the geometry of the decay chamber, we can find the average probability $\langle P[\tilde{\chi}_1^0 \text{ in d.r.}]\rangle$ of a neutralino decaying inside the detectable region. This is explained in more detail below.

A neutralino decaying inside the decay chamber is a necessary, but not a sufficient condition, as the final state particles have to be observed and traced back to an invisibly decaying new particle. For a charged final state, *e.g.* K^+e^-, one can measure the trajectory of both particles, measure their momenta and presumably identify the neutralino decay vertex. For a neutral final state, *e.g.* $K_L\nu$, one loses both the tracking information and the momentum of the second particle. We expect that these are hard to be linked to the decay of a neutralino. Thus we only count neutralinos that decay into charged

final state particles.[2] The final number of observed neutralinos is then

$$N_{\tilde{\chi}_1^0}^{\text{obs.}} = N_{\tilde{\chi}_1^0}^{\text{prod.}} \cdot \langle P[\tilde{\chi}_1^0 \text{ in d.r.}]\rangle \cdot \text{BR}(\tilde{\chi}_1^0 \to \text{charged})\,. \quad (56)$$

With the above considerations, we thus demand the following for observable neutralino decays via LQD operators at SHiP:

1. A pseudoscalar meson M with $m_M > m_{\tilde{\chi}_1^0}$ must have a non-vanishing decay rate into neutralinos.

2. The neutralino must have a non-vanishing decay rate into another charged meson $M'^{\pm}$ with $m_{M'^{\pm}} < m_{\tilde{\chi}_1^0} < m_M$.

With these this conditions, it is practically impossible for SHiP to observe R-Parity violation if only one λ'_{iab} coupling is nonzero. Eqs. (43)–(50) show which operator leads to which sets of mesons that can decay into the neutralino or the neutralino can decay into. The only operator related to both a pseudoscalar meson M and a charged meson $M'^{\pm}$ with $m_M > m_{M'^{\pm}}$ is λ'_{112}, which might be observable via the chain

$$K_{L/S}^0 \to \tilde{\chi}_1^0 \nu, \qquad \tilde{\chi}_1^0 \to K^{\pm}\ell^{\mp}\,. \quad (57)$$

However, as $|m_{K^{\pm}} - m_{K_{L/S}^0}| \approx 4$ MeV, the testable range of neutralino masses is extremely limited and the expected energies of the final state particles are so small that the decays would be very challenging to observe.

Thus we require two different operators $\lambda'_{iab}, \lambda'_{jcd} \neq 0$, with iab and jcd such that the decays fulfill the above requirements. This necessary extension leads to a plethora of possible combinations. In Sect. VIII we restrict ourselves to an interesting subset of benchmark scenarios.

VII. SIMULATION OF RPV SCENARIOS

Eqs. (55), (56) tell us how to estimate the number of observable neutralino decays $N_{\tilde{\chi}_1^0}^{\text{obs}}$ for any given operator combination and parameter values. The total widths and branching ratios into charged final states can be calculated from the general width formulae, Eqs. (38)-(41). We next describe the numerical tools we use to estimate N_M and $\langle P[\tilde{\chi}_1^0 \text{ in d.r.}]\rangle$.

To get a reliable estimate on the kinematics of the initially produced mesons at SHiP, as well as the resulting neutralinos after their decay, we use `Pythia 8.175` [69, 70]. In scenarios with initial charm (bottom) mesons we use the `HardQCD:hardccbar` (`HardQCD:hardbbbar`) matrix element calculator within `Pythia`, which includes the partonic processes $q\bar{q}, gg \to c\bar{c}\,(b\bar{b})$ and select the specific meson type for each benchmark scenario. According to [71], the number of $c\bar{c}$ events after 5 years of operation is expected to be $N_{c\bar{c}} = 9 \times 10^{16}$. By simulating 1M events of type $c\bar{c}$, we can use `Pythia` to find the average number of produced charm mesons per $c\bar{c}$ event, *i.e.*

$$n_D^{c\bar{c}} \equiv N_D / N_{c\bar{c}}, \;\; \text{with} \;\; D \in \{D^{\pm}, D_s\}\,. \quad (58)$$

The analogous simulation of $b\bar{b}$ events gives the respective number for bottom mesons:

$$n_B^{b\bar{b}} \equiv N_B / N_{b\bar{b}}, \;\; \text{with} \;\; B \in \{B^0, B^{\pm}, B_s^0\}\,. \quad (59)$$

The total number of expected $b\bar{b}$ events is taken by scaling the known number for $c\bar{c}$ events by the ratio of total cross sections determined by `Pythia`, *i.e.* $N_{b\bar{b}} = N_{c\bar{c}} \times \sigma_{b\bar{b}}/\sigma_{c\bar{c}}$. We therefore combine

$$N_M = N_{c\bar{c}} \cdot \begin{cases} n_M^{c\bar{c}} & \text{for charm mesons} \\ n_M^{b\bar{b}} \cdot \sigma_{b\bar{b}}/\sigma_{c\bar{c}} & \text{for bottom mesons} \end{cases} \quad (60)$$

and list the numerical values in Table II.

$N_{c\bar{c}}$	9×10^{16}
$\sigma_{b\bar{b}}/\sigma_{c\bar{c}}$	2.1×10^{-4}
$n_{D^{\pm}}^{c\bar{c}}$	0.53
$n_{D_s^{\pm}}^{c\bar{c}}$	0.074
$n_{B^{\pm}}^{b\bar{b}}$	0.83
$n_{B^0}^{b\bar{b}}$	0.80
$n_{B_s^0}^{b\bar{b}}$	0.14

TABLE II. Numerical values used to estimate the number N_M in Eq. (60). Except for $N_{\bar{c}c}$, which is taken from [71], all numbers are evaluated by simulating 1M events of each `HardQCD` type in `Pythia`.

For each benchmark scenario, we simulate 20,000 events of the correct `HardQCD` type and — to increase statistics — set the branching ratio $\text{BR}(M \to \tilde{\chi}_1^0 f)$ to 100 %. We then scale our results accordingly. As the decaying mesons are scalar particles, the momentum of the neutralino is chosen to be uniformly distributed in the rest frame of the decaying meson. We then sum over all produced neutralinos and determine the average probability, *i.e.* for all possible neutralino momenta, that an arbitrary neutralino decays within the SHiP detector. Given the four-vector of the neutralino $(\tilde{\chi}_1^0)_i$ in spherical coordinates as $(E_i, p_i^z, \theta_i, \phi_i)$ and the distances and angles as defined in Fig. 2, the average probability for $N_{\tilde{\chi}_1^0}^{\text{MC}}$ neutralinos in a given sample generated by a Monte Carlo program is evaluated as

$$\langle P[\tilde{\chi}_1^0 \text{ in d.r.}]\rangle = \frac{1}{N_{\tilde{\chi}_1^0}^{\text{MC}}} \sum_{i=1}^{N_{\tilde{\chi}_1^0}^{\text{MC}}} P[(\tilde{\chi}_1^0)_i \text{ in d.r.}], \quad (61)$$

$$P[(\tilde{\chi}_1^0)_i \text{ in d.r.}] = e^{-L_{t\to d}/\lambda_i^z} \cdot \left(1 - e^{-L_i/\lambda_i^z}\right). \quad (62)$$

[2] We note that this assumption has not been made in [30] and as such, our results for the same scenario slightly differ.

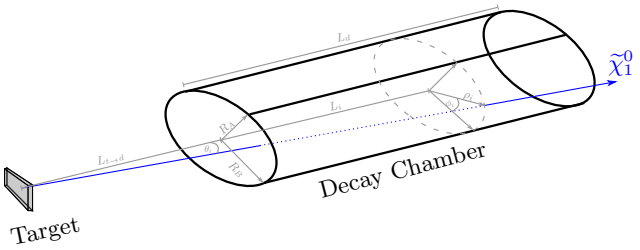

FIG. 2. Schematic overview of the SHiP detector geometry and definition of distances and angles used in text.

The mean decay length λ_i^z of the neutralino in the lab frame is given by

$$\lambda_i^z = \beta_i^z \gamma_i / \Gamma_{\rm tot}(\tilde{\chi}_1^0), \tag{63}$$

$$\beta_i^z = p_i^z / E_i, \tag{64}$$

$$\gamma_i = E_i / m_{\tilde{\chi}_1^0}. \tag{65}$$

β_i^z is the z-component of the relativistic velocity of $(\tilde{\chi}_1^0)_i$, γ_i the corresponding Lorentz boost factor. $\Gamma_{\rm tot}(\tilde{\chi}_1^0)$ is the total decay width of the neutralino LSP, which only depends on the model parameters and not on the kinematics of an individual candidate $(\tilde{\chi}_1^0)_i$. L_i denotes the distance in z-direction a neutralino can travel inside the decay chamber before leaving it in radial direction. It can be determined as, see also Fig. 2,

$$L_i = \begin{cases} 0 & \text{if } \rho_i \cot\theta_i < L_{t\to d}, \\ L_d & \text{if } \rho_i \cot\theta_i > L_{t\to d} + L_d, \\ \rho_i \cot\theta_i - L_{t\to d} & \text{else,} \end{cases} \tag{66}$$

$$\rho_i = R_A R_B / \sqrt{(R_B \cos\phi_i)^2 + (R_A \sin\phi_i)^2}. \tag{67}$$

ρ_i is the radius of the ellipse in the direction ϕ_i. θ_i is the angle between the flight direction of the neutralino and the central axis of the detector; the polar angle, ϕ_i, is the azimuthal angle of the neutralino momentum 3-vector. R_A denotes the semi-minor axis, and R_B the semi-major axis of the elliptical face of the detector. $L_{t\to d}$ denotes the distance from the target to the front of the detector. L_d denotes the length of the detector along the central axis. As explained in Sec. IV A, we use the numerical values $L_{t\to d} = 68.8$ m, $L_d = 55$ m, $R_A = 2.5$ m and $R_B = 5$ m.

VIII. RESULTS FOR VARIOUS BENCHMARK SCENARIOS

In Eqs. (43)-(50) we have listed the twenty-seven operators λ'_{iab} together with the corresponding mesons they couple to. For a fixed lepton flavor there are 36 possible combinations for production and decay of the neutralinos, if we assume distinct operators. The number of possibilities exceeds 100 if one in addition tests all possible values for the lepton flavor indices. It is clear that we can not investigate all of these cases in detail. In order to analyze the sensitivity at SHiP, we have thus focussed on a subset which we propose as, hopefully representative, benchmark scenarios.

In choosing the benchmark scenarios, we took the following points into consideration. For the sensitivity, to first order, it does not matter if we consider electrons or muons. We thus restrict ourselves to electrons.[3] We have one benchmark with final state taus, as their considerably larger mass affects the accessible decay phase space and the respective total widths.

The meson production rates can differ substantially. Thus we consider various scenarios where the neutralinos are produced via neutral or charged D- or B-mesons. To estimate the production rates we use `Pythia`, as discussed above. We do not consider the production of neutralinos via $\lambda'_{i11}, \lambda'_{i12}$ as the production of the corresponding light mesons are not well simulated in forward direction with `Pythia`. We postpone this to future work. For kinematic reasons, we restrict the final state mesons in the neutralino decays to K and D mesons. We also do not consider decays into pions and the associated vector resonances, as we expect sizable deviations from our approximations. However, from the results of the benchmark scenarios discussed below, an estimate for pion final states can be derived easily, by letting the neutralino mass range down to the pion mass of about 135 MeV, instead of the kaon mass. The pion and kaon decay constants are related by $SU(3)$ flavor symmetry. Of course, a neutralino decay into pions requires turning on the coupling λ'_{i11} where $i = 1, 2$. Note that in this case it does matter if $i = 2$ as now $m_\mu \simeq m_\pi$.

To be precise we consider the following cases, which we propose as benchmarks.

A. Benchmark Scenario 1

λ'_P for production	λ'_{121}
λ'_D for decay	λ'_{112}
produced meson(s)	$D^\pm$
visible final state(s)	$K^{(*)\pm} e^\mp$
invisible final state(s) via λ'_P	$(K_L^0, K_S^0, K^*) + (\nu, \bar{\nu})$
invisible final state(s) via λ'_D	$(K_L^0, K_S^0, K^*) + (\nu, \bar{\nu})$

TABLE III. Features of Benchmark Scenario 1.

We begin with scenarios where the neutralino is produced via the RPV decay of a D meson and subsequently decays into a kaon plus lepton. This scenario has already been studied in some detail (by two of us, HD, DS) in Ref. [30]. We turn on two RPV couplings λ'_{121}

[3] Although the bounds on λ'_{2jk} are typically weaker than on λ'_{1jk}.

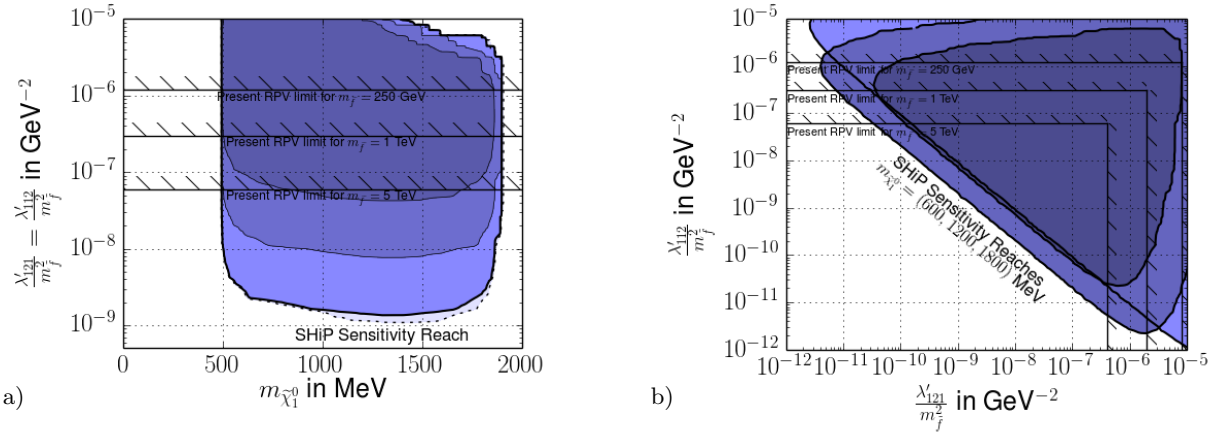

FIG. 3. SHiP sensitivity curves for Benchmark Scenario 1. In a), the two couplings are set equal. The maximum sensitivity reach, corresponding to ≥ 3 events, is shown in bright blue, with a solid curve edge. The blue area corresponds to $\geq 3 \cdot 10^3$ events and dark blue to $\geq 3 \cdot 10^6$ events. The dashed curve extending just below the light blue region denotes the extended sensitivity if the neutral mesons from neutralino decays are also visible. The horizontal hashed lines correspond to the existing limits on the RPV couplings, for three different sfermion masses: 250 GeV, 1 TeV, 5 TeV. In b), the sensitivity reach is shown as a function of the two independent RPV couplings for three fixed neutralino masses: 600 MeV (bright blue), 1200 MeV (blue), 1800 MeV (dark blue). For the x-axis we always choose the coupling responsible for the production of the neutralinos, here $\lambda'_{121}/m^2_{\tilde{f}}$. For the y-axis we choose the coupling responsible for the decay of the neutralinos, here $\lambda'_{112}/m^2_{\tilde{f}}$. The existing bounds on the RPV couplings are again shown as solid hashed lines for 3 different sfermion masses: 250 GeV, 1 TeV, 5 TeV.

and λ'_{112}. Neutralino production then occurs via the decay $D^{\pm} \to \tilde{\chi}^0_1 + e^{\pm}$ which is proportional to $(\lambda'_{121})^2$. The same coupling also leads to neutralino decay via the process $\tilde{\chi}^0_1 \to (K^0_L, K^0_S, K^{*0}) + \nu$ which contains no charged particles in the final state and will therefore be difficult to observe. However, these decays do impact the neutralino lifetime. The relevant information is summarized in Table III.

Because we have turned on the coupling λ'_{112} the neutralino can furthermore decay via $\tilde{\chi}^0_1 \to (K^{\pm}, K^{*\pm}) + e^{\mp}$, which is possible to detect at SHiP. This coupling also leads to the same invisible decay to neutral kaons and neutrinos as λ'_{121}. The invisible decays are important to include in the computation.

We now present our results. The expected number of events depends on three independent parameters: $\lambda'_{121}/m^2_{\tilde{f}}$, $\lambda'_{112}/m^2_{\tilde{f}}$, and the neutralino mass $m_{\tilde{\chi}^0_1}$. We find it convenient to present our results in two different ways. At first, we assume the RPV coupling constants to be equal, $\lambda'_{121} = \lambda'_{112} \equiv \lambda'$. In Fig. 3a) we show the number of expected visible neutralino decays in the SHiP detector as event rate iso-curves which are functions of $\lambda'/m^2_{\tilde{f}}$ and $m_{\tilde{\chi}^0_1}$. The bright blue area bounded by a thick solid line shows the expected maximum sensitivity curve for the SHiP experiment. This area in parameter space gives rise to ≥ 3 neutralino decays within the detector into charged final state particles for $2 \cdot 10^{20}$ protons-on-target. The corresponding expected meson production rates are listed in Sec. VII. To show how the event rate increases with $\lambda'/m^2_{\tilde{f}}$ and $m_{\tilde{\chi}^0_1}$, we also show areas for $\geq 3 \cdot 10^3$ (blue) and $\geq 3 \cdot 10^6$ (dark blue) observable decays. The horizontal hashed lines depict existing bounds on the couplings for various values of the sfermion mass $m_{\tilde{f}}$, *cf.* Sect. II B.

We see that the SHiP experiment can improve the current bounds on $\lambda'/m^2_{\tilde{f}}$ by one to three orders of magnitude depending on $m_{\tilde{f}}$. The kinematically accessible range for $m_{\tilde{\chi}^0_1}$ is dictated by the requirements that the neutralino must be lighter than the D-meson, yielding an upper bound, while at the same time being heavier than the K-meson, thus giving a lower bound. We find that the discovery region is mostly independent of $m_{\tilde{\chi}^0_1}$, *i.e.* the lower solid curve edge of the discovery range is fairly flat, as long as the mass lies within this kinematically allowed range between 500 and 1900 MeV.

The additional small lighter shaded region marked by the dashed line indicates the extended sensitivity if the SHiP detector could detect neutral kaons in the final state, as well. In this particular scenario, this barely affects the exclusion contours because the branching ratios to visible and invisible final states are roughly the same. However, as we see below, in other scenarios the difference can be more substantial.

If $\lambda'/m^2_{\tilde{f}}$ becomes larger than $10^{-5}\,\text{GeV}^{-2}$, the neutralinos decay too fast, in fact mostly before reaching the detector. We note that this parameter region is subject to large numerical uncertainties in our Monte Carlo simulation approach, and as such the exclusion lines show fluctuations with no underlying physical cause. In Fig. 3b) we remove the restriction that the couplings λ'_{121} and λ'_{112} are equal. Instead, we present the SHiP sensitivity depending on the separate couplings for three representative values of $m_{\tilde{\chi}^0_1}$. We choose a light mass close to the lower kinematic threshold (600 MeV, bright blue), a heavy one close to the higher kinematic threshold (1800 MeV, dark blue) and one halfway between the

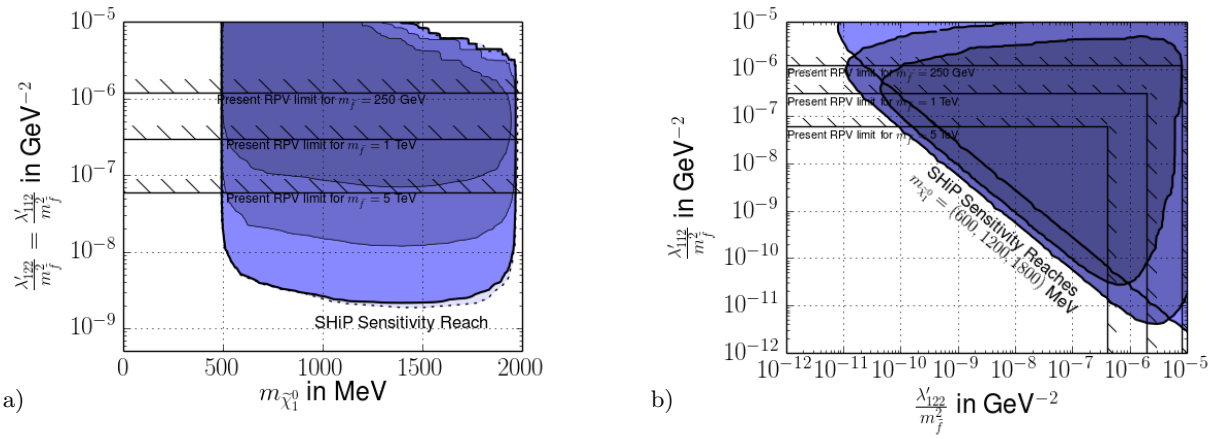

FIG. 4. Search sensitivity for Benchmark Scenario 2. The labelling is as in Fig. 3, except for the couplings λ'_{112}, λ'_{122}.

other two (1200 MeV, blue). In the same manner as before, existing limits on the two couplings are plotted for three representative values of $m_{\tilde{f}}$. Again we see that the contours are fairly insensitive to the neutralino mass. In all cases, SHiP probes a new region of parameter space even for 5 TeV sfermion masses. The shape of the sensitivity regions are due to *both* couplings defining the neutralino lifetime, but only λ'_{121} leads to the production and only λ'_{112} to the *observable* decay of the neutralinos. To avoid confusion, let us call the couplings λ'_P and λ'_D respectively in the following discussion. If $\lambda'_P/m^2_{\tilde{f}}$ becomes too small, too few neutralinos are produced in the first place. This leads to an overall minimum requirement on $\lambda'_P/m^2_{\tilde{f}}$.

For increasing $\lambda'_P/m^2_{\tilde{f}}$, more neutralinos are produced and thus the allowed neutralino lifetime to observe 3 events at SHiP can be reached for increasingly larger ranges of $\lambda'_D/m^2_{\tilde{f}}$. As before, too small/large couplings lead to too many neutralinos decaying after/before the detector. Furthermore, smaller λ'_D/λ'_P ratios lead to more invisibly decaying neutralinos. In Fig. 3b) this corresponds to the slanted edge running from the upper left-hand corner to the lower right-hand corner.

Once $\lambda'_P/m^2_{\tilde{f}}$ becomes too large, the lifetime induced by this operator is already too small and neutralinos decay mostly before reaching the detector, regardless of $\lambda'_D/m^2_{\tilde{f}}$. This explains the sensitivity limitations on the right edge of Fig. 3b.

The analysis described here applies to the cases:

$$\text{Production: } \lambda'_{i21}, \quad \text{Decay: } \lambda'_{j12}, \quad i,j \neq 3\,. \tag{68}$$

Note that for $i = 2$, neutralinos are produced via $D^\pm \to \widetilde{\chi}^0_1 + \mu^\pm$ and the extra muon would shift the upper kinematical limit of all regions in Fig. 3 by $m_\mu \approx 100\,\text{MeV}$ to the left. Analogously, the case $j = 2$ would move the lower kinematical limit of all but the shaded regions by the same amount to the right. Within this scenario, the cases $i = 3$ and/or $j = 3$ would not be observable as there would not be enough phase space to produce a τ lepton.

If SHiP is sensitive also to neutral final states, the above results also apply to the cases

$$\text{Production: } \lambda'_{i21}, \quad \text{Decay: } \lambda'_{j21}, \quad i,j \neq 3\,. \tag{69}$$

The sensitivity curve in this case would be very similar to the shaded region in Fig. 3a).

B. Benchmark Scenario 2

λ'_P for production	λ'_{122}
λ'_D for decay	λ'_{112}
produced meson(s)	D_s
visible final state(s)	$K^\pm e^\mp, K^{*\pm} e^\mp$
invisible final state(s) via λ'_P	$(\eta, \eta', \phi) + (\nu, \bar{\nu})$
invisible final state(s) via λ'_D	$(K^0_L, K^0_S, K^*) + (\nu, \bar{\nu})$

TABLE IV. Features of Benchmark Scenario 2.

This is similar to the previous benchmark, except the production of the neutralinos is via D_s mesons. The observable charged final states are the same. There are however further invisible neutral final states, which are kinematically accessible: $(\eta, \eta', \phi) + (\nu, \bar{\nu})$. The details of this benchmark scenario are summarized in Table IV.

The results for the SHiP sensitivity are presented in Fig. 4a). The reach is extended to higher neutralino masses, as $M_{D_s} > M_D$. The lower edge is still given by $m_{\tilde{\chi}^0_1} \approx M_K$. The sensitivity in $\lambda'/m^2_{\tilde{f}}$ is slightly weaker for two reasons. First, the production rate D_s mesons is lower than $D^\pm$ mesons, see Table II. Second, the neutralino branching ratio to an observable charged final state is smaller. Correspondingly the sensitivity is enhanced more in this scenario if neutral mesons are observable at SHiP, shown by the dashed line in the bottom of Fig. 4b).

Analogously to Benchmark Scenario 1, the analysis described here applies to the cases

$$\text{Production: } \lambda'_{i22}, \quad \text{Decay: } \lambda'_{j12}, \quad i,j \neq 3\,. \tag{70}$$

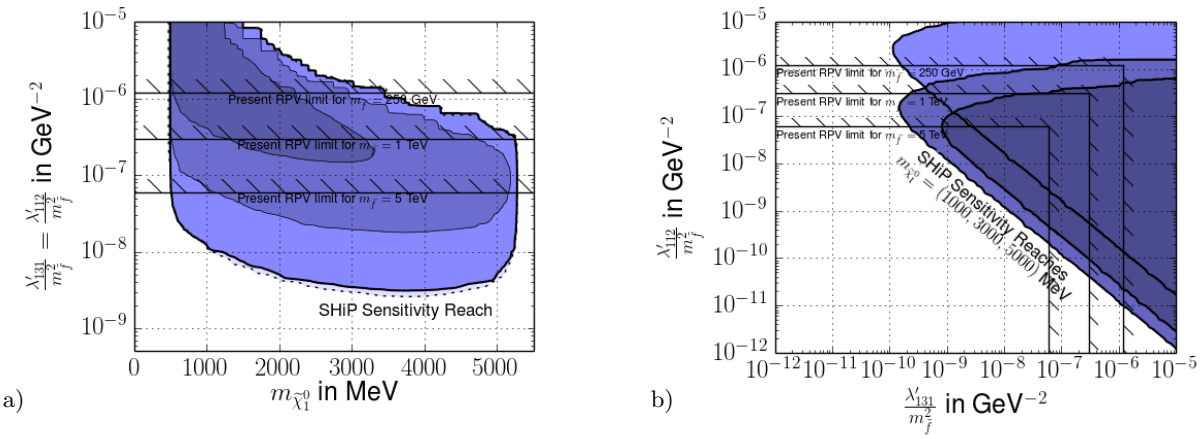

FIG. 5. Search sensitivity for Benchmark Scenario 3. The labelling is as in Fig. 3, except for the couplings λ'_{112}, λ'_{131}. Also in b) the neutralino masses are 1000 MeV (light blue), 3000 MeV (blue), and 5000 MeV (dark blue). Note that the x-axis range for figure a) has been changed compared to previous cases, as the initial state B meson allows for a larger kinematical reach.

If the neutral final-state mesons are visible, it also applies to the cases

$$\text{Production: } \lambda'_{i22}, \quad \text{Decay: } \lambda'_{j21}, \lambda'_{j22}, \quad i,j \neq 3\,. \tag{71}$$

C. Benchmark Scenario 3

λ'_P for production	λ'_{131}
λ'_D for decay	λ'_{112}
produced meson(s)	$B^0, \bar{B}^0$
visible final state(s)	$K^{\pm}e^{\mp}, K^{*\pm}e^{\mp}$
invisible final state(s) via λ'_P	none
invisible final state(s) via λ'_D	$(K^0_L, K^0_S, K^*) + (\nu, \bar{\nu})$

TABLE V. Features of Benchmark Scenario 3

In this scenario the neutralino production is via B mesons. The decay of the neutralino via the coupling λ'_{112} leads to charged K-mesons and electrons, which are readily visible. The coupling λ'_{112} also leads to neutral neutralino decays to K^0 mesons and neutrinos. There are no additional kinematically accessible invisible neutralino decay modes through the coupling λ'_{131}. This information is summarized in Table V.

The results of the simulation in this scenario are presented in Fig. 5. The kinematically accessible neutralino mass range is $M_{K^\pm} < m_{\tilde{\chi}^0_1} < M_{B^0}$. This is reflected in the shape of the sensitivity region in Fig. 5a), which is cut off on the left at a neutralino mass of about 500 MeV and on the right just under 5.3 GeV. In the top-right corner, where $\lambda'/m^2_{\tilde{f}}$ and $m_{\tilde{\chi}^0_1}$ are large, the neutralino lifetime becomes very short. The neutralinos then overwhelmingly decay before the detector. Since so few neutralinos reach the detector, we are here probing the extreme tail of the exponential decay distribution. Consequently, the top-right part of the curve is jagged, due to lack of statistics in this regime. The lower curve slopes downward left to right, much more so than in Figs. 3a) and 4a). This effect is due to the presence of the final-state vector mesons (K^*), which are more important for the heavier neutralinos, accessible in B-meson decays. This is discussed in more detail in Section VIII G, below. The added sensitivity due to possible neutral final states is marginal, as the branching ratios are comparable.

As can be seen from the numbers in Table II, the B-meson production rate is roughly four orders of magnitude smaller than the D-meson production rate. As the neutralino production is proportional to $(\lambda'/m^2_{\tilde{f}})^2$, the curves in Fig. 5b) are shifted by almost two orders of magnitude to the right, compared to the corresponding results, *e.g.* Fig. 3b), of the previous benchmark scenarios. The new sensitivity reach of SHiP is thus smaller here. However, since λ'_{131} does not induce any invisible decays of the neutralino, the sensitivity regions in Fig. 5b) are not bounded on the right, in contrast to analogous regions of previous scenarios. Increasing $\lambda'_{131}/m^2_{\tilde{f}}$ then always leads to an increased number of expected neutralinos and hence always improves the sensitivity to $\lambda'_{112}/m^2_{\tilde{f}}$. We note that Fig. 5b) has the same characteristic shape as Fig. 6 in Ref. [26].

The analysis described here applies to the cases

$$\text{Production: } \lambda'_{i31}, \lambda'_{i13}, \quad \text{Decay: } \lambda'_{j12}, \quad i,j \neq 3\,. \tag{72}$$

Again, if neutral final state mesons can be observed it also applies to the cases

$$\text{Production: } \lambda'_{i31}, \lambda'_{i13}, \quad \text{Decay: } \lambda'_{j21}, \quad i,j \neq 3\,. \tag{73}$$

Although as we discuss below in Section VIII D, in this case there are additional charged decay modes via D-mesons.

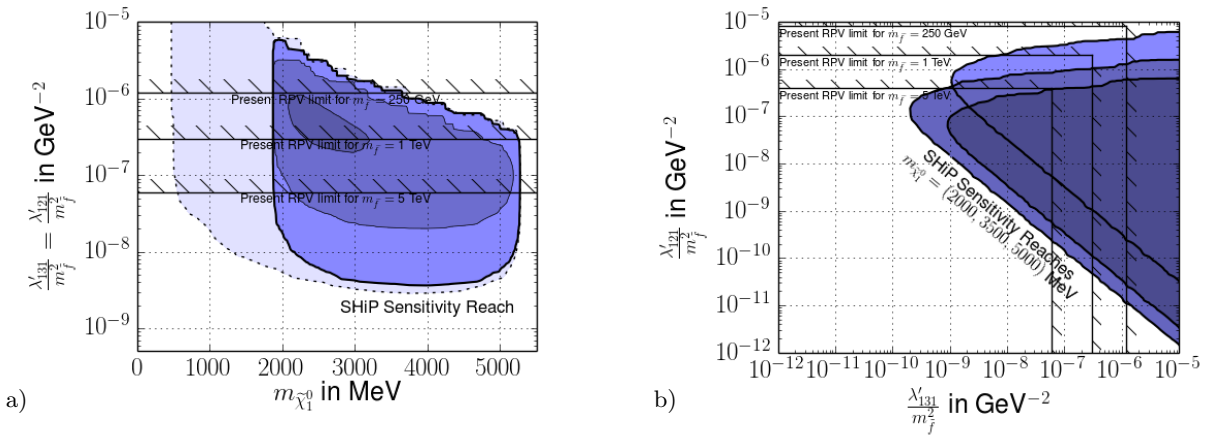

FIG. 6. Search sensitivity for Benchmark Scenario 4. The labelling is as in Fig. 3 except for the couplings λ'_{131}, λ'_{121}. Also in b) the neutralino masses are 2000 MeV (light blue), 3500 MeV (blue), and 5000 MeV (dark blue).

D. Benchmark Scenario 4

λ'_P for production	λ'_{131}
λ'_D for decay	λ'_{121}
produced meson(s)	$B^0, \bar{B}^0$
visible final state(s)	$D^{\pm}e^{\mp}, D^{*\pm}e^{\mp}$
invisible final state(s) via λ'_P	none
invisible final state(s) via λ'_D	$(K^0_L, K^0_S, K^*) + (\nu, \bar{\nu})$

TABLE VI. Features of Benchmark Scenario 4

In this scenario the neutralinos are also produced via B-mesons and the coupling λ'_{131}. However, now the decay is into D mesons via the coupling λ'_{121}. There are kinematically accessible invisible decays to neutral K mesons and neutrinos via λ'_{121} This is summarized in Table VI.

The results of the simulation for this scenario are displayed in Fig. 6. In the left panel, we show the search sensitivity as a function of the neutralino mass and of a common coupling $\lambda'_{113}/m^2_{\tilde{f}} = \lambda'_{112}/m^2_{\tilde{f}} \equiv \lambda'/m^2_{\tilde{f}}$. The mass sensitivity range is again mainly fixed kinematically: $M_D < m_{\tilde{\chi}^0_1} < M_B$, which is narrower than in Fig. 5 due to the larger D-meson mass.

When allowing for neutral final states the sensitivity is dramatically increased to lower neutralino masses, corresponding to the kinematic range $M_K < m_{\tilde{\chi}^0_1} < M_B$. This is shown in Fig. 6a) by the very light blue region bounded by the dashed line.

In Fig. 6b) the sensitivity range is similar to Fig. 5b), as it is dominated by B-meson production. The differences in the curves are mainly due to the different neutralino masses that are considered: 2000 MeV (light blue), 3500 MeV (blue), and 5000 MeV (dark blue).

The analysis described here also applies to the cases

$$\text{Production: } \lambda'_{i31},\ \lambda'_{i13}, \quad \text{Decay: } \lambda'_{j21} \quad i,j \neq 3\,. \tag{74}$$

E. Benchmark Scenario 5

λ'_P for production	λ'_{313}
λ'_D for decay	λ'_{312}
produced meson(s)	$B^0, \bar{B}^0, B^{\pm}(+\tau^{\mp})$
visible final state(s)	$K^{\pm}\tau^{\mp}, K^{*\pm}\tau^{\mp}$
invisible final state(s) via λ'_P	none
invisible final state(s) via λ'_D	$(K^0_L, K^0_S, K^*) + (\nu, \bar{\nu})$

TABLE VII. Features of Benchmark Scenario 5. At the end of the third row we emphasize that the charged B-meson decay to the neutralino is accompanied by a tau.

Here the production goes via B-mesons and the coupling λ'_{313}. We thus consider the third generation lepton index. The features of this benchmark scenario are summarized in Table 7. At the end of the third row, the $(+\tau^{\pm})$ indicates that the charged B-meson decay to a neutralino is accompanied by a tau,

$$B^{\pm} \to \tilde{\chi}^0_1 + \tau^{\pm}\,. \tag{75}$$

Therefore the charged $B^{\pm}$ meson can only contribute for the restricted neutralino mass range $m_{\tilde{\chi}^0_1} < M_B - m_{\tau}$. The corresponding *neutral* B-meson decay has neutrinos in the final state and is thus allowed for the larger range $m_{\tilde{\chi}^0_1} < M_B$. In Fig. 7a) this leads to a kink in the solid curves surrounding the sensitivity regions at $m_{\tilde{\chi}^0_1} = M_B - m_{\tau}$. The region corresponding to $\geq 10^6$ events is also cut off to higher neutralino masses compared to Fig. 6a).

The neutralino decay proceeds via the coupling λ'_{312}.

$$\tilde{\chi}^0_1 \to K^{\pm} + \tau^{\mp}\,. \tag{76}$$

Thus the visible final states involve charged K-mesons *and* tau leptons, which might be difficult to detect, especially in the hadronic decay mode. This also requires $m_{\tilde{\chi}^0_1} > M_K + m_{\tau} \simeq 2300\,\text{MeV}$. This is the cutoff on the left of the blue regions in Fig. 7a).

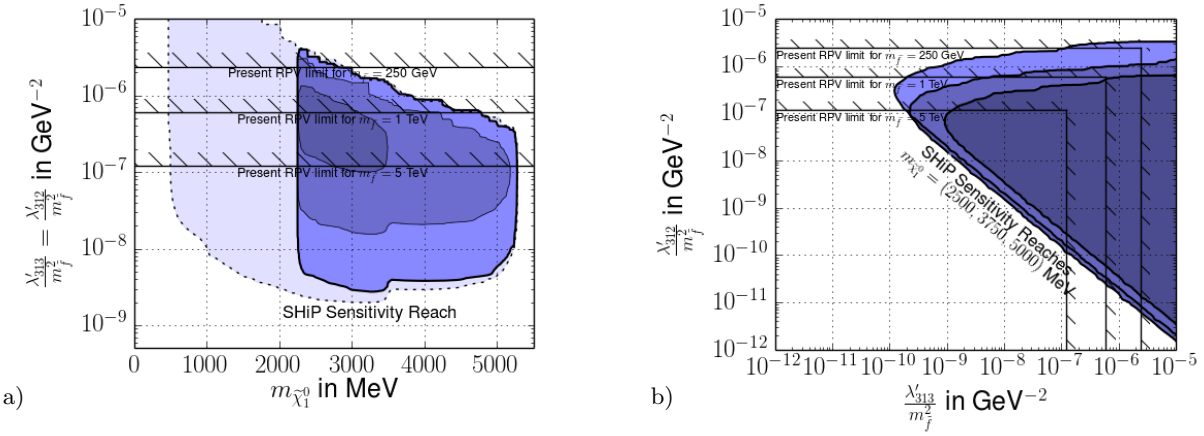

FIG. 7. Search sensitivity for Benchmark Scenario 5. The labelling is as in Fig. 3 except for the couplings λ'_{313}, λ'_{312}. Also in b) the neutralino masses are 2750 MeV (light blue), 3750 MeV (blue), and 5000 MeV (dark blue).

There are possible additional neutral final states involving neutral K-mesons and neutrinos and *no* tau lepton. When these are included the sensitivity reach is dramatically extended to lower neutralino masses as can be seen in Fig. 7a), just as in Fig. 6a).

Fig. 7b) shows the sensitivity region as a function of the two now independent couplings $\lambda'_{313}/m^2_{\tilde{f}}$ and $\lambda'_{312}/m^2_{\tilde{f}}$ for the three neutralino masses 2750 MeV (light blue), 3750 MeV (blue), and 5000 MeV (dark blue). These are slightly modified compared to Scenario 4, because of the tau mass, leading to slightly different curves.

The analysis described here applies to the cases

$$\text{Production: } \lambda'_{i13},\ \lambda'_{i31}, \quad \text{Decay: } \lambda'_{j12} \tag{77}$$

with either i or j or both equal to 3. In case of λ'_{i31} only neutral B-mesons can decay into a neutralino and corresponding neutrino such that the sensitivity curves are independent of i. The curves look similar to those in Fig. 7, but the kink around $M_B - m_\tau \simeq 3500$ MeV does not appear. The case $j = 1$ leads to similar limits as the dashed region drawn in Fig. 7b), whereas similarly to previous scenarios it is shifted by m_μ to the right for $j = 2$.

F. Related Scenarios

As we have seen the sensitivity curves are largely shaped by the kinematics. There are thus some related scenarios which we briefly describe here. Benchmark scenarios 3, 4 and 5 are easily extended to the cases

$$\text{Production: } \lambda'_{i32},\ \lambda'_{i23}, \tag{78}$$

by considering the production via B_s mesons. As can be seen from Table II, B_s production is suppressed compared to B-meson production by roughly a factor $n^{b\bar{b}}_{B^0}/n^{b\bar{b}}_{B^0_s} \approx 0.18$. The sensitivity to the coupling $\lambda'/m^2_{\tilde{f}}$ is reduced by roughly a factor $\sqrt[4]{0.18} \approx 0.65$.

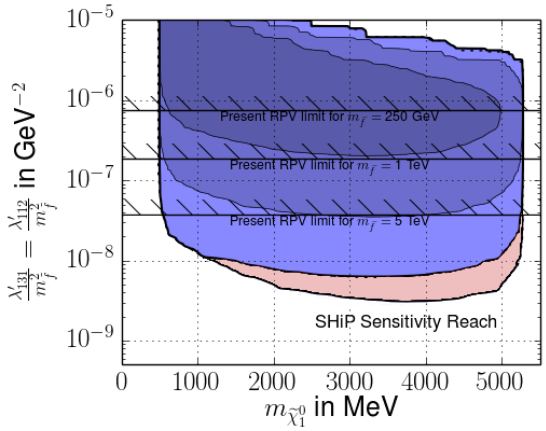

FIG. 8. Sensitivity curve for enchmark Scenario 3 if decays into vector mesons are ignored. The pink region shows the sensitivity curve including vector mesons which corresponds to the "SHiP sensitivity reach" of Fig. 5a)

.

Similarly the decay in Scenarios 4 and 5 are easily extended to the cases $\lambda'_D = \lambda'_{122}$, where D_s mesons appear in the final state. This gives rise to very similar sensitivity curves, the only difference being a slightly larger lower-mass reach for the neutralino.

G. Relevance of Vector Mesons

As discussed at the end of Sec. V A, the inclusion of vector mesons in the final state leads to a reduced sensitivity to potential fine-tuning of the SUSY parameters. As discussed at the end of Sec. V A, the inclusion of vector mesons in the final state lead to complementary dependence on SUSY paramaters. In addition, the final state vector mesons lead to an interesting kinematical enhancement of the neutralino de-

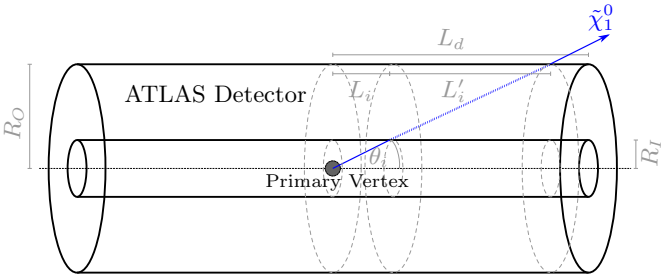

FIG. 9. Schematic overview of the ATLAS detector geometry and definition of distances and angles used in text.

cay width. This enhancement can be understood from the decay width formulæ in Eqs. (40) and (41). When $m_{\tilde{\chi}_1^0} \gg m_M$, where m_M is the mass of the final state meson, the decay to scalar mesons is proportional to $(f_M^S)^2 m^2_{\tilde{\chi}_1^0} \simeq f_M^2 m_M^2 m^2_{\tilde{\chi}_1^0}$, whereas the decay to vector mesons is proportional to $(f_M^T)^2 m^4_{\tilde{\chi}_1^0} \simeq f_M^2 m^4_{\tilde{\chi}_1^0}$. The decay into vector mesons is thus enhanced by roughly a factor $m^2_{\tilde{\chi}_1^0}/m_M^2$.

This is mainly relevant for cases such as our Benchmark Scenario 3, where neutralino production occurs via B-meson decays. Then the neutralino can be significantly heavier than the final-state meson, here the kaon. To illustrate the enhancement, in Fig. 8, we repeat the analysis for Benchmark Scenario 3, but exclude final state vector mesons. The sensitivity contour of the same analysis including vector mesons is shown by the pink shaded area. This region is identical to the sensitivity area shown in Fig. 6a). We show it again here to make the difference between the two cases easier to see. The inclusion of vector mesons is barely visible for neutralino masses smaller than 1 GeV, but the enhancement is clearly visible in the 2-5 GeV mass range.

IX. LHC ESTIMATE

As we have seen, the sensitivity at SHiP in the production coupling results from an interplay between the length scales of the target- detector-distance $L_{t\to d}$, the length of the detector L_d, the meson production rate N_M, the boost γ_i of the neutralinos and their azimuthal angle θ_i. The LHC operates at much higher energies in the center-of-mass frame and the detectors are built right at the collision points. Thus all the above parameters change and we would expect a different sensitivity when comparing to SHiP[4]. To estimate the net result of these effects, we thus here briefly discuss the sensitivity for our scenarios at the LHC.

To allow for an easy comparison, we consider two example cases which correspond to our earlier discussed

[4] We thank Jesse Thaler for drawing our attention to this point. See also [72] on a related discussion on dark photons.

$N_{c\bar{c}}$	1.5×10^{15}
$\sigma_{b\bar{b}}/\sigma_{c\bar{c}}$	8.6×10^{-3}
$n^{c\bar{c}}_{D^\pm}$	0.59
$n^{b\bar{b}}_{B^\pm}$	0.87
$n^{b\bar{b}}_{B^0}$	0.87

TABLE VIII. Numerical values used to estimate the number N_M in Eq. (60) for the LHC with $\sqrt{s} = 14$ TeV and an integrated luminosity of 250 fb^{-1}. All numbers are evaluated by simulating 1M events of each `HardQCD` type in `Pythia`.

Benchmark Scenarios 1 and 5. These involve the observable decay chains

$$D^\pm \to \tilde{\chi}_1^0 e^\pm, \quad \tilde{\chi}_1^0 \to e^\pm K^\mp \quad \text{via } \lambda'_{121}, \lambda'_{112}, \tag{79}$$
$$B^\pm/B^0 \to \tilde{\chi}_1^0 \tau^\pm/\nu, \quad \tilde{\chi}_1^0 \to \tau^\pm K^\mp \quad \text{via } \lambda'_{313}, \lambda'_{312}. \tag{80}$$

To compare like with like, we estimate the neutralino event rates analogously to Sec. VII: we simulate these scenarios using `Pythia 8.175` [69, 70], and find a production cross section for $c\bar{c}$ at 14 TeV of $6 \cdot 10^{12}$ fb and $\sigma_{b\bar{b}}/\sigma_{c\bar{c}} = 8.6 \times 10^{-3}$. We consider an integrated luminosity of 250 fb^{-1}, which roughly corresponds to the expected value for a high-energy LHC running for 5 years. We determine the other parameters of interest as in Sec. VII and list them in Table VIII.

As an example we consider the ATLAS detector setup as sketched in Fig. 9. Here we assume the detectable region to approximately range from $R_I = 0.0505$ m, the beginning of the inner detector, to $R_O = 11$ m, the end of the muon chambers. The detector has cylindrical shape with a total length of $2L_D = 43$ m. The probability for the neutralino to decay within this range is then, similarly to Eq. (62),

$$P[(\tilde{\chi}_1^0)_i \text{ in d.r.}] = e^{-L_i/\lambda_i^z} \cdot \left(1 - e^{-L_i'/\lambda_i^z}\right), \tag{81}$$
$$L_i \equiv \min(L_d, |R_I/\tan\theta_i|) \tag{82}$$
$$L_i' \equiv \min(L_d, |R_O/\tan\theta_i|) - L_i \tag{83}$$

with angles and distances defined in Fig. 9 and λ_i^z as defined in Eq. (63). In similar manner as for SHiP, we use `Pythia` to simulate 20,000 events, force all mesons of the right type to decay into neutralinos and average the results for $P[(\tilde{\chi}_1^0)_i$ in d.r.] over all these Monte-Carlo neutralinos to find the overall probability that an LHC-produced neutralino decays inside the detectable region of the ATLAS detector. The number of observable neutralino decays is then determined by considering the RPV branching ratio of the initially produced mesons and the branching ratio of neutralinos into charged final states, according to Eqs. (55), (56).

The expected sensitivity regions are shown in Fig. 10. For easy comparison we show the same information as in their corresponding SHiPs analogues Figs. 6a) and 7a) and focus on the 3 event threshold which would be

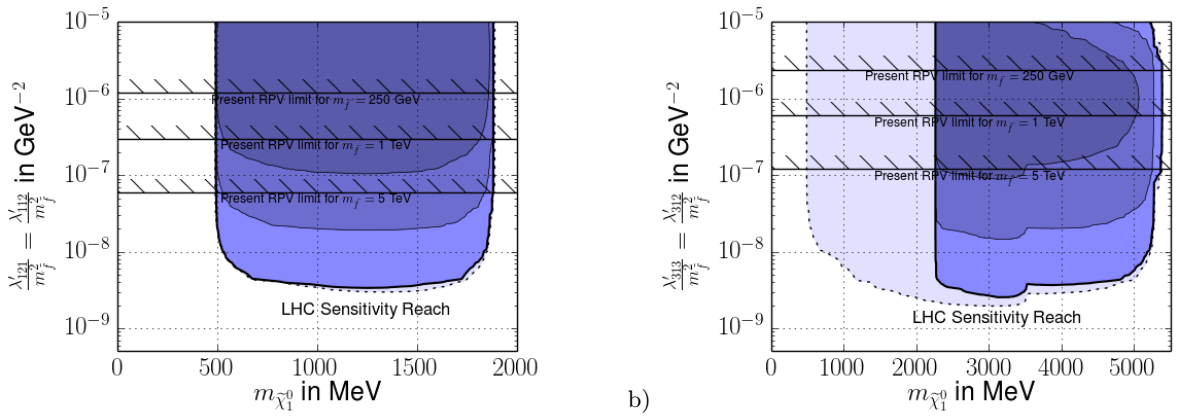

FIG. 10. Expected LHC search sensitivity for a) Benchmark Scenario 1 and b) Benchmark Scenario 5. The labelling is as in Figs. 3,7.

required for a significant observation. We restrict the discussion to the $m_{\tilde{\chi}^0_1}$–$\lambda'/m^2_{\tilde{f}}$–plane as the limits in the $\lambda'_{\text{prod.}}/m^2_{\tilde{f}}$–$\lambda'_{\text{dec.}}/m^2_{\tilde{f}}$–plane can be easily deduced.

For both scenarios, the structure of the plots do not largely differ between ATLAS and SHiP. The testable kinematic regions are obviously identical for the same scenario and it is only the required value for $\lambda'/m^2_{\tilde{f}}$ to observe enough neutralino decays which changes. At SHiP we found that the expected sensitivity quickly drops if the neutralinos decay too promptly, that is before they reach the decay chamber at roughly 70 m behind the target. This resulted in an upper limit on the couplings SHiP would be sensitive to. However, as the detectable region at ATLAS already starts at $\mathcal{O}$(cm) distances from the primary vertex, this upper limit is pushed to higher values.

Comparing the results for Scenario 1, Figs. 6a) and 10a), we find that LHC has a comparable but still by a factor 2 weaker expected sensitivity on $\lambda'/m^2_{\tilde{f}}$ than the expected value from SHiP. From comparing the respective values for $N_{c\bar{c}}$ in Tables VIII and VIII, one expects SHiP to produce almost 100 times more neutralinos than the LHC in a comparable time frame. This is partially compensated by the effect that neutralinos which are produced at large angles θ can be observed at the almost spherical ATLAS detector but miss the decay chamber at SHiP.

Furthermore, the boost distribution of the two experiments largely differ. The fixed target setup of SHiP causes most produced mesons to have a large boost which is inherited by the daughter neutralinos they decay into. Contrarily, the center-of-mass collision for the LHC will lead to most mesons to be produced at rest. We show the boost distribution of the neutralinos we get with `Pythia` in Fig. 11. For SHiP, the distribution shows an expectation value of $\langle\gamma\rangle \approx 30$ and a maximum probability for $\gamma_{\text{max}} \approx 7.5$. This leads to an increased lifetime in the lab frame which reduces the detection probability if $c\tau_\chi$ is larger than the size of the detector, see *e.g.* Eq. (62).

The large center-of-mass energy of the LHC leads to an even larger *average* boost, $\langle\gamma\rangle \approx 55$, which however has a larger spread, resulting in many neutralinos with boost of $\mathcal{O}(1)$ and a few with boost $\mathcal{O}(1000)$. As shown in Fig. 11, the peak of the boost distribution for the LHC is located at $\gamma = 2.5$ and the resulting large fraction of unboosted neutralinos improve the overall probability to observe a decay within ATLAS.

Combining the above effects, we find that $\langle P[\tilde{\chi}^0_1 \text{ in d.r.}]\rangle$ at ATLAS is greater by a factor 4 than at SHiP. Taking into account the much larger meson production yield of SHiP, it is expected to observe approximately 25 times more events than ATLAS, leading to an improved sensitivity on the coupling of $\sqrt[4]{25} \approx 2.2$.

For Scenario 5, we compare Figs. 7a) and 10b) and interestingly find very comparable expected sensitivities. All the effects discussed for the previous scenario equally apply here and lead to approximately similar results. Therefore one would still expect SHiP to observe roughly 25 times more decays. However, this scenario requires B-mesons to be initially produced. The larger center-of-mass energy at LHC leads to an increased relative production yield $\sigma_{b\bar{b}}/\sigma_{c\bar{c}}$ of approximately 40 (see Tables II, VIII). This results in a roughly 60 % larger overall expected event rate at the LHC, which however is a negligible improvement when translated into a limit on $\lambda'/m^2_{\tilde{f}}$.

It is clear that the results we show can just serve as a very approximate comparison. As we do not know the efficiency with which SHiP would be able to detect a neutralino decay and distinguish it from Standard Model, we did not take it into account for our LHC discussion either. However, it can be expected that the final state efficiencies for the two experiments differ significantly, most likely with a significant penalty on the ATLAS side. SHiP will be specifically designed to observe rare decays of new, long-lived particles. It can therefore be expected that the neutralino decays will have a large probability to actually be measured by the detector. The ATLAS detector, however, is not designed for this purpose. The combined

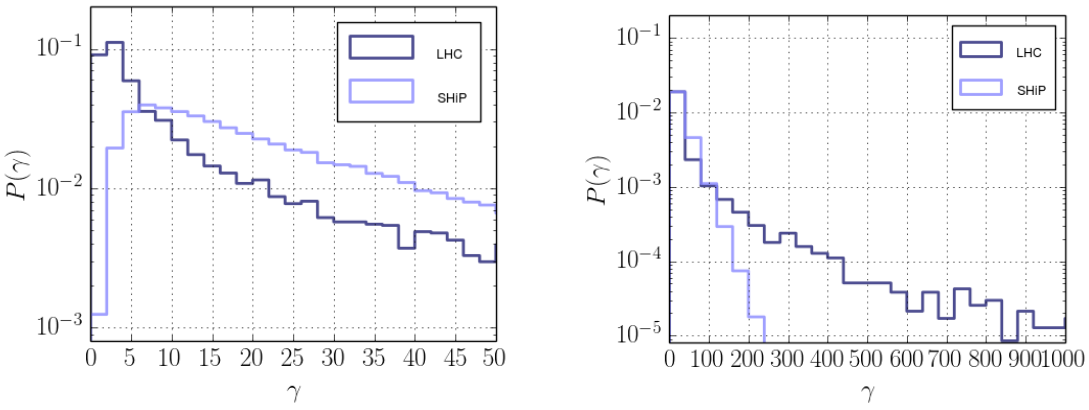

FIG. 11. Boost distribution for neutralinos produced at a $\sqrt{s} = 14$ TeV LHC and at SHiP, determined with `Pythia`. We show the same results for two different choices of axis scaling. The fluctuations for $\gamma \gtrsim 300$ are caused by limited Monte Carlo statistics.

efficiencies to trigger on the event, to reconstruct the final state particles, to identify the significantly displaced vertex and to distinguish it from Standard Model mesons decays will most likely lead to a significant reduction of the final event yield, potentially by orders of magnitude. Still, we find it an interesting observation that when just considering the geometry of the setup, the meson production yield and the expected kinematics of the neutralinos, SHiP and ATLAS seem to have comparable sensitivity to the discussed decay scenario. Thus we conclude that the final state reconstruction efficiency will play a crucial role in determining the importance of the SHiP experiment with regards to the search for light neutralinos.

X. SUMMARY

In this work we have studied the sensitivity of the proposed SHiP experiment to the R-parity violating production and decay of neutralinos whose masses lie in the range of $0.5 - 5$ GeV. As discussed in Sect. III, a neutralino in this mass range is only allowed if R-parity is violated. We have focused on the semi-leptonic R-parity violating operators $\lambda' LQ\bar{D}$, but our work is easily extended to the purely leptonic case $\lambda LL\bar{E}$. The basic idea pursued in this work is that a small fraction of the D and B mesons produced in the SHiP experiment, can potentially decay into a neutralino plus lepton. Because the R-parity violating couplings are expected to be small, the neutralino can have a sufficiently long lifetime to travel a distance of 63.8 m to the ShiP detector where it can subsequently decay into a, presumably detectable, meson-lepton pair.

For neutralinos in the mass-range of $0.5 - 5$ GeV, the SHiP experiment is sensitive to several combinations of R-parity violating couplings. In general, the number of neutralino decays in the SHiP detector is proportional to $(\lambda'_{iab}\lambda'_{jcd})^2/m^8_{\tilde{f}}$, where i, j denote the lepton generation indices and a, b, c, d the quark generation indices. We have classified benchmark scenarios for different combinations of the generation indices i, j, a, b, c, d. Although many different combinations of couplings exist, we have argued that most of them can be captured in this relatively small set of benchmark scenarios. We highlight here a number of conclusions and caveats of our findings.

- We find no feasible scenario where SHiP is sensitive to only a single λ'_{iab} coupling. The main obstacle for such a scenario is that the final state decay products will consist of a neutrino and a neutral meson from which it is difficult to reconstruct the neutralino decay. An example of such a scenario would be a nonzero λ'_{i21} coupling, which would lead to the production and decay channels $D^{\pm} \to \tilde{\chi}^0_1 + l^{\pm}_i$ and $\tilde{\chi}^0_1 \to K_{S,L} + \nu$. In order to get an observable final state we thus always require two distinct nonzero λ' couplings. We have found, however, that including the invisible final states is mandatory as they influence the neutralino lifetime.

- That being said, we have shown that the SHiP experiment has the potential to significantly improve the constraints on various combinations of R-parity violating couplings. This is clearly illustrated in the figures in Sect. VIII. For instance, constraints on $\lambda'_{112}/m^2_{\tilde{f}}$ can be strengthened by one to three orders of magnitude (see Fig. 3), depending on the sfermion mass. Similar improvements are found for third generation couplings such as $\lambda'_{131}\lambda'_{121}/m^4_{\tilde{f}}$. We have presented sensitivity curves for each of the benchmark scenarios: $[\lambda'_{121}, \lambda'_{112}]$, $[\lambda'_{122}, \lambda'_{112}]$, $[\lambda'_{131}, \lambda'_{112}]$, $[\lambda'_{131}, \lambda'_{121}]$, $[\lambda'_{313}, \lambda'_{312}]$. These curves can be used to estimate the sensitivity of the SHiP experiment to various combinations of R-parity violating interactions, as outlined in the text.

- We have focused on neutralino production via the decay of B and D mesons. Very light neutralinos

could be produced in kaon decays and be detected by their subsequent decay into pionic final states. We have not included this in this work as the production of light mesons is not well simulated in the forward direction with `Pythia`. We aim to study this in future work as it would extend the sensitivity to the neutralino mass range $0.1 - 0.5$ GeV. Similarly, we plan to include neutralino production in the decays of $\bar{b}b$ mesons, which would give a sensitivity to λ'_{i33} and to higher-mass neutralinos.

- We have found that including vector mesons in the final state leads to an enhanced sensitivity to neutralinos at the higher end of the allowed mass range. This enhancement can be understood from the decay-width formula presented in Sect. V B as discussed in Sect. VIII G. In addition, the neutralino decay into vector mesons is proportional to a different combination of SUSY parameters than the corresponding decay into scalar mesons. The processes are therefore complementary.

- Our analysis did not include possible uncertainties arising from hadronic matrix elements. The decay constants used are not in all cases known to high precision. Nevertheless, the SHiP sensitivity curves range over many orders of magnitude and we do not expect that changes in the decay constants drastically change our conclusions.

- We determined the expected sensitivity of the ATLAS detector at a 14 TeV LHC with an integrated luminosity of $250\,\mathrm{fb}^{-1}$. To do a fair comparison, we did not take into account the final state reconstruction efficiency and only determined the expected number of neutralino decays inside the detector region of ATLAS. We found that in scenarios with initially produced D mesons, ATLAS expects roughly 4 % of the number of events expected for SHiP, leading to an expected limit on $\lambda'/m^2_{\tilde{f}}$ which is weaker by roughly a factor of 2. This is caused by a combination of a larger meson flux expected for SHiP and a higher detection probability for long-lived neutralinos at ATLAS. For initially produced B mesons, the expected sensitivities are very similar, as the large LHC energies will produce relatively more b-quarks. It is therefore the final state reconstruction efficiency which will be the decisive factor.

Note added

While completing this work, a related study appeared [73]. They consider the production via B-mesons as in [26] and the decay to kaons or purely leptonically. They make extensive use of the formulæ in the original study as presented by two of us (HKD and DS) in [30], and thus employs the error we made there, as discussed here in footnote 1.

ACKNOWLEDGMENTS

This work (JdV) is supported in part by the DFG and the NSFC through funds provided to the Sino-German CRC 110 "Symmetries and the Emergence of Structure in QCD" (Grant No. 11261130311). We thank Christoph Hanhart for several useful discussions. We thank Jesse Thaler for drawing our attention to the possibility of searching for these scenarios at the LHC. One of us (HD) thanks the Galileo Galilei Institut in Florence for hospitality, where a significant part of this work was completed.

[1] J. Wess and B. Zumino, Nucl. Phys. **B70**, 39 (1974).
[2] H. P. Nilles, Phys.Rept. **110**, 1 (1984).
[3] S. P. Martin, (1997), arXiv:hep-ph/9709356 [hep-ph].
[4] R. Haag, J. T. Lopuszanski, and M. Sohnius, Nucl. Phys. **B88**, 257 (1975).
[5] E. Gildener, Phys. Rev. **D14**, 1667 (1976).
[6] M. Veltman, Acta Phys. Polon. **B12**, 437 (1981).
[7] P. Bechtle *et al.*, JHEP **06**, 098 (2012), arXiv:1204.4199 [hep-ph].
[8] H. Baer, V. Barger, P. Huang, D. Mickelson, A. Mustafayev, *et al.*, Phys.Rev. **D87**, 115028 (2013), arXiv:1212.2655 [hep-ph].
[9] M. W. Cahill-Rowley, J. L. Hewett, A. Ismail, and T. G. Rizzo, Phys. Rev. **D86**, 075015 (2012), arXiv:1206.5800 [hep-ph].
[10] G. G. Ross, K. Schmidt-Hoberg, and F. Staub, JHEP **08**, 074 (2012), arXiv:1205.1509 [hep-ph].
[11] D. M. Ghilencea, Phys. Rev. **D89**, 095007 (2014), arXiv:1311.6144 [hep-ph].
[12] G. Aad *et al.* (ATLAS), Eur. Phys. J. **C75**, 318 (2015), arXiv:1503.03290 [hep-ex].
[13] V. Khachatryan *et al.* (CMS), JHEP **05**, 078 (2015), arXiv:1502.04358 [hep-ex].
[14] G. Aad *et al.* (ATLAS), JHEP **05**, 071 (2014), arXiv:1403.5294 [hep-ex].
[15] V. Khachatryan *et al.* (CMS), Phys. Rev. **D90**, 092007 (2014), arXiv:1409.3168 [hep-ex].
[16] H. K. Dreiner, S. Heinemeyer, O. Kittel, U. Langenfeld, A. M. Weber, and G. Weiglein, Eur. Phys. J. **C62**, 547 (2009), arXiv:hep-ph/0901.3485 [hep-ph].
[17] K. A. Olive *et al.* (Particle Data Group), Chin. Phys. **C38**, 090001 (2014).
[18] H. K. Dreiner, C. Hanhart, U. Langenfeld, and D. R. Phillips, Phys. Rev. **D68**, 055004 (2003), arXiv:hep-ph/0304289 [hep-ph].
[19] D. Choudhury, H. K. Dreiner, P. Richardson, and S. Sarkar, Phys. Rev. **D61**, 095009 (2000), arXiv:hep-ph/9911365 [hep-ph].

[20] H. K. Dreiner, O. Kittel, and U. Langenfeld, Phys. Rev. **D74**, 115010 (2006), arXiv:hep-ph/0610020 [hep-ph].

[21] H. K. Dreiner, O. Kittel, and U. Langenfeld, Eur. Phys. J. **C54**, 277 (2008), arXiv:hep-ph/0703009 [HEP-PH].

[22] D. Hooper and T. Plehn, Phys. Lett. **B562**, 18 (2003), arXiv:hep-ph/0212226 [hep-ph].

[23] A. Bottino, N. Fornengo, and S. Scopel, Phys. Rev. **D85**, 095013 (2012), arXiv:1112.5666 [hep-ph].

[24] G. Belanger, G. Drieu La Rochelle, B. Dumont, R. M. Godbole, S. Kraml, *et al.*, Phys.Lett. **B726**, 773 (2013), arXiv:1308.3735 [hep-ph].

[25] H. K. Dreiner, (1997), arXiv:hep-ph/9707435 [hep-ph].

[26] A. Dedes, H. K. Dreiner, and P. Richardson, Phys. Rev. **D65**, 015001 (2001), arXiv:hep-ph/0106199 [hep-ph].

[27] H. Dreiner, G. Polesello, and M. Thormeier, (2002), arXiv:hep-ph/0207160 [hep-ph].

[28] H. K. Dreiner, S. Grab, D. Koschade, M. Kramer, B. O'Leary, and U. Langenfeld, Phys. Rev. **D80**, 035018 (2009), arXiv:0905.2051 [hep-ph].

[29] M. Anelli *et al.* (SHiP), (2015), arXiv:1504.04956 [physics.ins-det].

[30] S. Alekhin *et al.*, (2015), arXiv:1504.04855 [hep-ph].

[31] G. R. Farrar and P. Fayet, Phys. Lett. **B76**, 575 (1978).

[32] H. K. Dreiner, C. Luhn, and M. Thormeier, Phys. Rev. **D73**, 075007 (2006), arXiv:hep-ph/0512163 [hep-ph].

[33] L. M. Krauss and F. Wilczek, Phys. Rev. Lett. **62**, 1221 (1989).

[34] H. Goldberg, Phys. Rev. Lett. **50**, 1419 (1983).

[35] L. E. Ibanez and G. G. Ross, Phys. Lett. **B260**, 291 (1991).

[36] E. J. Chun and H. B. Kim, Phys. Rev. **D60**, 095006 (1999), arXiv:hep-ph/9906392 [hep-ph].

[37] D. Hooper and L.-T. Wang, Phys.Rev. **D70**, 063506 (2004), arXiv:hep-ph/0402220 [hep-ph].

[38] H. K. Dreiner, F. Staub, and L. Ubaldi, Phys. Rev. **D90**, 055016 (2014), arXiv:1402.5977 [hep-ph].

[39] S. Colucci, H. K. Dreiner, F. Staub, and L. Ubaldi, Phys. Lett. **B750**, 107 (2015), arXiv:1507.06200 [hep-ph].

[40] L. J. Hall and M. Suzuki, Nucl. Phys. **B231**, 419 (1984).

[41] E. Nardi, Phys. Rev. **D55**, 5772 (1997), arXiv:hep-ph/9610540 [hep-ph].

[42] M. Hirsch, M. A. Diaz, W. Porod, J. C. Romao, and J. W. F. Valle, Phys. Rev. **D62**, 113008 (2000), [Erratum: Phys. Rev.D65,119901(2002)], arXiv:hep-ph/0004115 [hep-ph].

[43] H. K. Dreiner, C. Luhn, H. Murayama, and M. Thormeier, Nucl. Phys. **B774**, 127 (2007), arXiv:hep-ph/0610026 [hep-ph].

[44] H. K. Dreiner, M. Hanussek, J.-S. Kim, and C. H. Kom, Phys. Rev. **D84**, 113005 (2011), arXiv:1106.4338 [hep-ph].

[45] H. K. Dreiner and M. Thormeier, Phys. Rev. **D69**, 053002 (2004), arXiv:hep-ph/0305270 [hep-ph].

[46] V. D. Barger, G. F. Giudice, and T. Han, Phys. Rev. **D40**, 2987 (1989).

[47] G. Bhattacharyya, in *Beyond the desert 1997: Accelerator and non-accelerator approaches. Proceedings, 1st International Conference on Particle Physics beyond the Standard Model, Tegernsee, Ringberg Castle, Germany, June 8-14, 1997* (1997) arXiv:hep-ph/9709395 [hep-ph].

[48] B. Allanach, A. Dedes, and H. K. Dreiner, Phys. Rev. **D60**, 075014 (1999), arXiv:hep-ph/9906209 [hep-ph].

[49] R. Barbier, C. Berat, M. Besancon, M. Chemtob, A. Deandrea, *et al.*, Phys.Rept. **420**, 1 (2005), arXiv:hep-ph/0406039 [hep-ph].

[50] Y. Kao and T. Takeuchi, (2009), arXiv:0910.4980 [hep-ph].

[51] T. Banks, Y. Grossman, E. Nardi, and Y. Nir, Phys. Rev. **D52**, 5319 (1995), arXiv:hep-ph/9505248 [hep-ph].

[52] H. K. Dreiner, H. E. Haber, and S. P. Martin, Phys.Rept. **494**, 1 (2010), arXiv:hep-ph/0812.1594 [hep-ph].

[53] M. Kachelriess, JHEP **02**, 010 (2000), arXiv:hep-ph/0001160 [hep-ph].

[54] H. K. Dreiner, J.-F. Fortin, J. Isern, and L. Ubaldi, Phys. Rev. **D88**, 043517 (2013), arXiv:1303.7232 [hep-ph].

[55] R. Cowsik and J. McClelland, Phys. Rev. Lett. **29**, 669 (1972).

[56] B. W. Lee and S. Weinberg, Phys. Rev. Lett. **39**, 165 (1977).

[57] J. M. Lindert, F. D. Steffen, and M. K. Trenkel, JHEP **08**, 151 (2011), arXiv:1106.4005 [hep-ph].

[58] L. Calibbi, J. M. Lindert, T. Ota, and Y. Takanishi, JHEP **10**, 132 (2013), arXiv:1307.4119.

[59] L. Calibbi, J. M. Lindert, T. Ota, and Y. Takanishi, JHEP **11**, 106 (2014), arXiv:1410.5730 [hep-ph].

[60] G. Corcella, I. G. Knowles, G. Marchesini, S. Moretti, K. Odagiri, P. Richardson, M. H. Seymour, and B. R. Webber, JHEP **01**, 010 (2001), arXiv:hep-ph/0011363 [hep-ph].

[61] M. Drees, R. Godbole, and P. Roy, *Theory and phenomenology of Sparticles: an account of four-dimensional N=1 supersymmetry in high-energy physics* (World Scientific, Singapore, 2004).

[62] C. M. Bouchard, (2011).

[63] N. Isgur and M. B. Wise, Phys. Lett. **B232**, 113 (1989).

[64] H. Dreiner, M. Kramer, and B. O'Leary, Phys.Rev. **D75**, 114016 (2007), arXiv:hep-ph/0612278 [hep-ph].

[65] R. Casalbuoni, A. Deandrea, N. Di Bartolomeo, R. Gatto, F. Feruglio, and G. Nardulli, Phys. Rept. **281**, 145 (1997), arXiv:hep-ph/9605342 [hep-ph].

[66] T. Feldmann, P. Kroll, and B. Stech, Phys. Rev. **D58**, 114006 (1998), arXiv:hep-ph/9802409 [hep-ph].

[67] S. Dawson, Nucl. Phys. **B261**, 297 (1985).

[68] S. Aoki *et al.*, Eur. Phys. J. **C74**, 2890 (2014), arXiv:1310.8555 [hep-lat].

[69] T. Sjostrand, S. Mrenna, and P. Z. Skands, JHEP **05**, 026 (2006), arXiv:hep-ph/0603175 [hep-ph].

[70] T. Sjostrand, S. Mrenna, and P. Z. Skands, Comput. Phys. Commun. **178**, 852 (2008), arXiv:0710.3820 [hep-ph].

[71] W. Bonivento *et al.*, (2013), arXiv:1310.1762 [hep-ex].

[72] P. Ilten, J. Thaler, M. Williams, and W. Xue, (2015), arXiv:1509.06765 [hep-ph].

[73] D. Gorbunov and I. Timiryasov, Phys. Rev. **D92**, 075015 (2015), arXiv:1508.01780 [hep-ph].